Water Air Soil Pollut (2023) 234:349
https://doi.org/10.1007/s11270-023-06359-9

A Review on Photocatalysis Used For Wastewater Treatment: Dye Degradation

Harita Kumari · Sonia · Suman · Rohit Ranga · Surjeet Chahal · Seema Devi · Sourabh Sharma · Sandeep Kumar · Parmod Kumar · Suresh Kumar · Ashok Kumar · Rajesh Parmar

Received: 21 February 2023 / Accepted: 9 May 2023

Abstract Water pollution is a global issue as a consequence of rapid industrialization and urbanization. Organic compounds which are generated from various industries produce problematic pollutants in water. Recently, metal oxide (TiO_2, SnO_2, CeO_2, ZrO_2, WO_3, and ZnO)-based semiconductors have been explored as excellent photocatalysts in order to degrade organic pollutants in wastewater. However, their photocatalytic performance is limited due to their high band gap (UV range) and recombination time of photogenerated electron–hole pairs. Strategies for improving the performance of these metal oxides in the fields of photocatalysis are discussed. To improve their photocatalytic activity, researchers have investigated the concept of doping, formation of nanocomposites and core–shell nanostructures of metal oxides. Rare-earth doped metal oxides have the advantage of interacting with functional groups quickly because of the 4f empty orbitals. More precisely, in this review, in-depth procedures for synthesizing rare earth doped metal oxides and nonocomposites, their efficiency towards organic pollutants degradation and sources have been discussed. The major goal of this review article is to propose high-performing, cost-effective combined tactics with prospective benefits for future industrial applications solutions.

Keywords Metal oxides · Photocatalytic degradation · Rare earth dopants · Nanocomposites · Core–shell · Band gap tuning

1 Introduction

With the current economic development and population growth, protecting water resources is a pressing concern. Every day, about 2 million tons of waste pollutants are carelessly released into the public water supply, gravely affecting human health and resulting in numerous deaths (Yan et al., 2021).

Present Address:
H. Kumari · R. Parmar
Department of Physics, Maharshi Dayanand University, Rohtak 124001, Haryana, India

Present Address:
Sonia · Suman · R. Ranga · S. Kumar · A. Kumar (✉)
Department of Physics, Deenbandhu Chhotu Ram University of Science and Technology, Murthal 131039, Haryana, India
e-mail: ashokkumar.phy@dcrustm.org

S. Chahal
Materials and Nano Engineering Research Laboratory, Department of Physics, School of Physical Sciences, DIT University, Dehradun 248009, India

S. Devi · S. Sharma
Department of Physics, Netaji Subhas University of Technology, New Delhi 110078, India

S. Kumar · P. Kumar
J. C. Bose University of Science and Technology, YMCA, Faridabad 121006, Haryana, India

The most representative pollutants are residual toxic dyes, monoaromatic hydrocarbons, and antibiotics originating from industrial wastes, such as rhodamineB (RhB), 4-nitrophenol (4-NP), and naproxen (NPX), which exhibit thermal and photo-resistant stability. According to reports, the maximum amount of 4-NP in water should be kept to less than 10 ppb (Devi et al., 2023; Yang et al., 2020a). Every year, more than 175,000 tons of dyes and 54,000 tons of antibiotics are arbitrary released into worldwide water resources (He et al., 2019; Zhang et al., 2015). Concern has grown greatly and deeply as water pollution has become an intractable challenge. In fact, numerous methods of waste water purification, including ion-exchange techniques, adsorption, membrane separation techniques, and electrochemical purification, have been proposed and put into action to address the water resources (Li et al., 2021; Suman et al., 2020a, b). Although much efforts have been put towards solving this problem, there are still several obstacles, including limited adsorption capacity, ready inactivity, secondary pollutants, and high energy consumption. To address this challenging issue, photo-induced catalytic degradation technology has recently attracted a lot of attention (Feng et al., 2023). Solar energy is most environmentally friendly, cost-effective, and even endless source of energy. On the other hand, innovative semiconductor photocatalysts that use active radicals to degrade organic pollutants can be rationally designed and produced as a result of advancements in nanoscience and nanotechnology (He et al., 2019; Hu et al., 2019). Cost-effectiveness, environmental friendly nature, and minimal energy usage are further benefits of photocatalysis process (Huang et al., 2018; Wei et al., 2019; Wu et al., 2020). Despite semiconductor photocatalysis technology being a talent self-driving potential technique by harvesting inexhaustible solar energy, the efficiency of photocatalysts in converting solar energy is considerably lower than predicted. This is because it is challenging to discover a single photocatalyst that can absorb all of the solar energy while maintaining low recombination rates of photo-induced carriers and strong photo stability (Bie et al., 2019; Wei et al., 2018; Xu et al., 2019). Since the components of composite have some synergistic effects, it is believed that composite of co-photocatalysts will partially satisfy the difficult acquisition.

Many materials can be used for photocatalytic process, but metal oxides specifically titanium oxide (TiO_2), cerium oxide (CeO_2), zinc oxide (ZnO), zirconium oxide (ZrO_2), manganese oxide (MnO_2), and tin oxide (SnO_2) are considered as excellent photocatalysts in this class due to their high stability in wide pH range, higher efficiency, low-cost, easy availability, less toxicity, being eco-friendly, and highly oxidizing photo-generated holes (Alam et al., 2018; Keerthana et al., 2021; Shaheen et al., 2020; Singh et al., 2018). However, there are several drawbacks of utilizing these metal oxides for photocatalytic degradation, such as incomplete mineralization and a wide band gap (Vaiano et al., 2018; Wang et al., 2019), which significantly limit their photocatalytic activity. Furthermore, a significant factor in dye degradation is the quick transport of electrons and holes (Rani & Shanker, 2021; Xing, 2017). However, rapid recombination of electrons (e^-) and holes (h^+) greatly reduces their potential for photocatalytic degradation (Liu et al., 2019; Rani et al., 2019). Hence, photocatalytic effectiveness of pure metal oxides was not up to mark. So as to improve their efficiency, rare earth doped metal oxides, metal oxide nanocomposites, core–shell nanostructures of metal oxides, etc. have been investigated (Joshi et al., 2022; Shanmuganathan et al., 2020; Wahba et al., 2020). However, a wider variety of catalysts are described here to give a more comprehensive understanding of the materials utilized. These are classified into three categories: single metal oxide, doped, and composite photocatalysts.

1.1 Wastewater Sources

Water consisting of toxic heavy metals, microorganisms, organic materials, and soluble inorganic compounds are treated as sources of wastewater. These pollutants interfere with freshwater's chemical, biological, and physical properties (Abou El-Nour et al., 2010). Sources of wastewater can be classified mainly into three categories as shown in Fig. 1 (Adams et al., 2006). Further, different types of pollutants which are found in water are shown in Fig. 2. World Health Organization (WHO) estimates that more than 13.7 million deaths worldwide occurred in 2016 as a result of people working and living in unhealthy environment. Particularly, air pollution resulted in almost 6 million deaths, while water

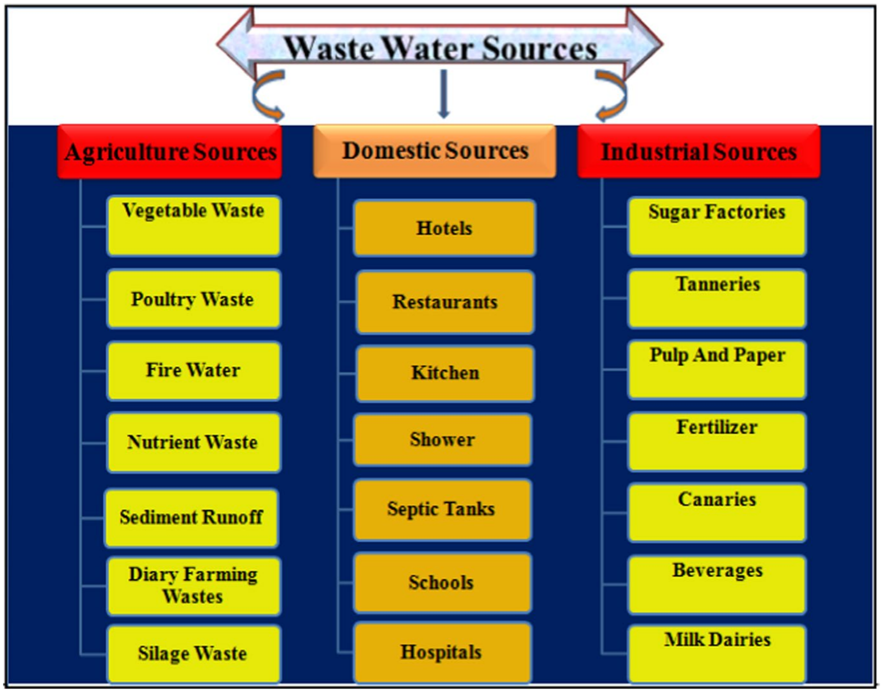

Fig. 1 Schematic representation of various wastewater sources

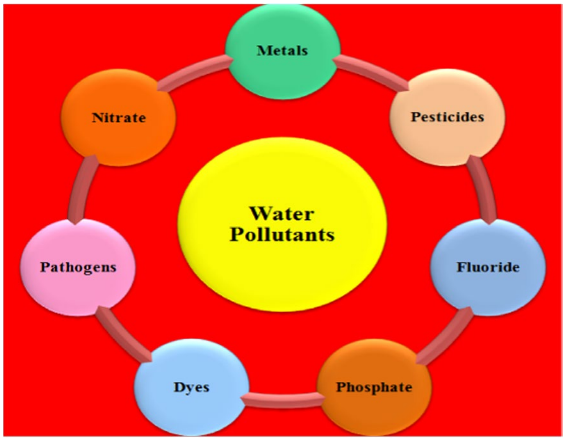

Fig. 2 Different types of pollutants found in water

contamination resulted in over 1.8 million deaths, demanding extensive remediation techniques (Dharwal et al., 2020; Kumar et al., 2021).

Nowadays, treatment of wastewater has become crucial due to the harmful impact of pollutants and risk of polluted wastewater on animals, human beings, as well as on agriculture. In order to protect the environment from contamination, effective actions must be taken at personal and government level for wastewater treatment. Physical, biological, and chemical procedures can be involved for the treatment of wastewater. Dye and other substances can be physical pollutants in wastewater (fixed, volatile, dissolved, and suspended). Wastewater may contain organic, inorganic, or gaseous substances as chemical pollutants. Figure 3 shows an overview of chemicals used by textile industries, which is the major source of water pollution. Along with physical and chemical characteristics biological characteristics are additionally prevalent in the contaminated water. Biological pollutants consist of pathogenic microorganisms like bacteria, protozoa, and viruses causing intense and chronic health impacts (Shon et al., 2007).

2 Textile Dyes and Their Impact on Environment

Contaminated water is a serious problem that has far-reaching consequences for the environment. Numerous insecticides, dyes, metal ions, chemical and inorganic substances, and other toxins pollute our environment. The non-biodegradable and potentially dangerous nature of dyes is largely attributable to the presence of stable aromatic rings in majority of

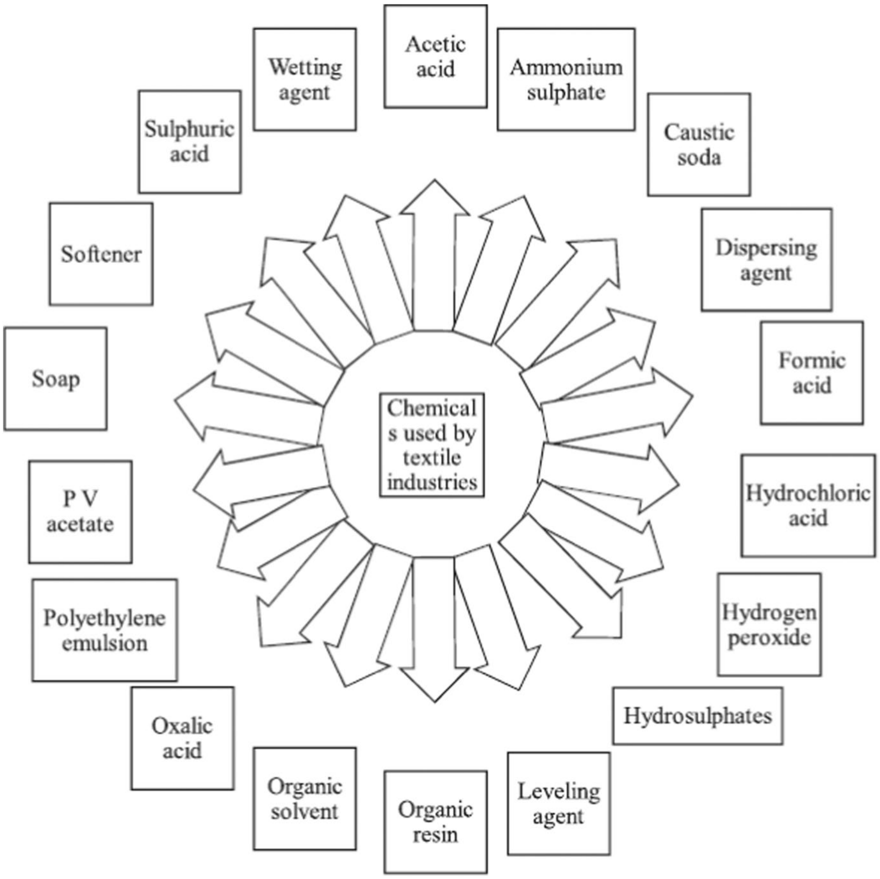

Fig. 3 Hazardous substances used by industries that utilize dyes (Katheresan et al., 2018)

dyes. Even a trace amount of dye can contaminate a system (Kapoor et al., 2021). Therefore, dye usage is one of the detrimental types of pollutants that need to be reduced in environment. Most of the dyes are stable in presence of light, heat, and oxidizers; hence, they are not biodegradable. Dyes have an effect on aquatic ecology because they alter the habitat's aesthetic value.

Dyes may be classified as cationic, anionic, and non-ionic. Dyes can also be categorized on the basis of functional groups: azo, indigo, phthalocyanine, anthraquinone, sulfur, etc. (Benkhaya et al., 2020). Dyes can be grouped together as basic, dispersed, vat, acidic, reactive, etc. For each color, textile dyes have interesting chemical structure (Solayman et al., 2023). Figure 4 presents many industries that are to blamed for the existence of dye effluents in atmosphere.

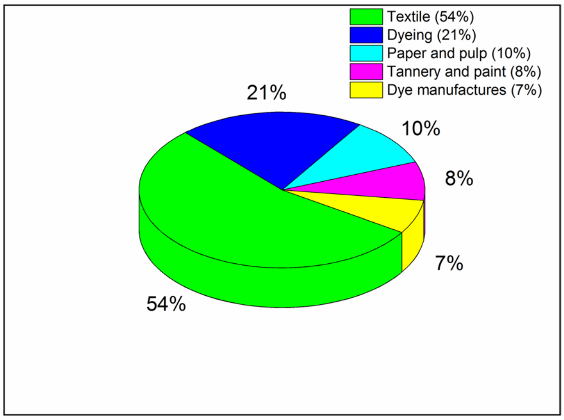

Fig. 4 Industries in charge of discharging dye effluent into the environment (Katheresan et al., 2018)

Every year, world creation of textile dyes is assessed in excess of 10,000 tons and roughly 100 tons of dyes are delivered to wastewater consistently (Semeraro et al., 2015). Not only that, but textile industry is currently most polluting in the entire globe. Therefore, textile production is biggest cause of adverse environmental effects (Lellis et al., 2019). Dyes have capability of absorbing light radiation in the range of visible region (380–700 nm).When white light reflects off a surface or is diffused or transmitted, it changes from white to colored light as a result of selective energy absorption by particular atoms (chromophoric groups). To put it another way, a dye is a substance with the capacity to absorb some light radiations and subsequently reflect complimentary colors. Before the middle of nineteenth century, natural materials like beet root were used as sources for dyes. The natural dyes might be acquired from insects, plants, minerals, and animals. Biodegradation can be utilized to treat wastewater produced by natural dyes as they are usually less hazardous and allergic than synthetic dyes (Sivakumar et al., 2009). Table 1 provides a general overview of the different dyes.

2.1 Motivation

In the upcoming future for upholding a better environment, fostering a better and sustainable ecosystem is an obligatory requirement. Because of industrial outlets, the environment gets polluted, resulting harmful health effects to human being, aquatic creatures, terrestrial animals, and plants. Because effluents from textile industry play a significant role in environmental pollution, we were inspired and motivated to take on task of authoring this review study. In order to establish a sustainable environment, this review article focuses on combining modern and classical approaches to remove pollutants from textile wastewater. To get rid of textile effluents, industrial wastewater is treated utilizing a number of chemical, biological, physical, and electrochemical techniques. The main focus of this article is on to explore the behavior of various dyes resulting from textile and pharmaceutical industries followed by their abatement using metal oxide–based photocatalysts.

3 Dye Removal Techniques

Many more dyes in addition to those listed in Table 1 also pose serious risks to human health and the ecosystem. The most dangerous ones are RB and phenol dyes. Over previous many years, various physical, chemical, and biological techniques like membrane filtration, precipitation, ion exchange, distillation, electrolysis, electrodialysis, flotation, conventional adsorption, ion exchange, chemical oxidation, biological treatment, ultrasonic-assisted adsorption, and chemical coagulation have been done to treat dye effluents and to eliminate dyes from aqueous solutions (Karimi-Maleh et al., 2020; Katheresan et al., 2018). Techniques for removing dye via physical, chemical, and biological means are illustrated in Fig. 5. Tables 2, 3, and 4 provide several physical, chemical, and biological dye removal strategies along with their benefits and drawbacks, accordingly.

Since we have a lot of methods for wastewater treatment, but highly efficient and cheaper methods need to be explored for providing safe water access to every human being. Among all these methods, photocatalysis has gained much attention since it is most effective and eco-friendly method till date. Photocatalytic frameworks with required band gap, high stability, large surface area, and suitable morphology are of extreme significance. The photocatalytic process can be carried out with a variety of different materials; however, TiO_2, SnO_2, CeO_2, ZrO_2, and ZnO are usually considered as most effective photocatalysts in this category.

4 Advanced Oxidation

Perovskite catalysts and advanced oxidation processes (AOPs) have been used in recent years to remove organic pollutants from wastewater. AOPs have been fully implemented in wastewater treatment, pharmaceutical industry, textiles, and general circular economy scale globally. AOPs can be divided into multiple categories based on various processes that generate free radicals. AOPs have been developed recently that differ in the ways to generate reactive oxygen species (ROS) and kinds of these species. Categorization of processes and applications mentioned in research can be used to evaluate the effect of each AOP separately, as well as in combination. Single AOPs may be used to purify and treat waste and wastewater at very efficient rates; however, combinations of AOPs have been implemented in many cases, with prominent results.

Basic classification of AOPs comprises of processes of UV/H_2O_2, Fenton and photo-Fenton, ozone-based (O_3) processes, photocatalysis,

Table 1 General information about dyes according to their color index, chromophore structure, and toxicity

Dye name	Structure	Chemical formula	Nature	Safety/toxicity	Appearance	Ref
Phenol	Carbolic acid	C_6H_6O	Acidic	Carcinogenicity, and mutagenicity	Transparent crystalline solid	Farhan Hanafi & Sapawe, 2020)
Methyl Orange	Benzenesulfonate	$C_{14}H_{14}N_3NaO_3S$	Acidic	Carcinogenicity, genotoxicity, mutagenicity	Orange-yellow powder or crystals	Mohammadi et al., 2011; Janbandhu et al., 2019)
Remazol Brilliant Blue	Disodium 1-amino-9	$C_{22}H_{16}N_2Na_2O_{11}S_3$	Acidic	Carcinogenicity, genotoxicity, mutagenicity	Dark blue crystalline powder	Soares et al., 2001)
Methylene Blue	Methylthioniniumchloride	$C_{16}H_{18}ClN_3S$	Basic	An eye irritant and may irritate skin	Dark green powder	Thevarajah et al., 2005; Chen et al., 2022)
Rose Bengal	4,5,6,7-Tetrachloro-2',4',5',7'-tetraiodo-fluorescein	$C_{20}H_4Cl_4I_4O_5$	Acidic	Carcinogenicity	Bright red stain	Demartis et al., 2021)
Rhodamine B	Diethylammonium Chloride	$C_{28}H_{31}ClN_2O_3$	Basic	Causes skin irritation	Red to violet powder	Al-Gheethi et al., 2022)
Congo Red	-	$C_{32}H_{22}N_6Na_2O_6S_2$	Acid–base indicator dye	Carcinogen and mutagen	Red-brown powder	Naseem et al., 2018)
Methyl Red	(2-(N,N-dimethyl-4-aminophenyl) azobenzenecarboxylic acid)	$C_{15}H_{15}N_3O_2$	Weak acidic	Cause headache, dizziness, drowsiness, and nausea	Dark red crystalline powder	Ahmad et al., 2019)
Direct Blue	4'-Diyl)bis(azo))bis(5-amino-4-hydroxy)-2	$C_{34}H_{24}N_6Na_4O_{16}S_4$	-	Causes mutation	Dark blue solid	Hernández-Zamora, 2087)
Acid Violet 7	N-(4-aminophenyl) acetamide	$C_{20}H_{16}N_4$ $Na_2O_9S_2$	Acidic	Causes degradation of lipid, chromosomal abnormality	Violet powder. Deep red powder	Ben Mansour et al., n.d.)
Reactive Brilliant Red	Disodium;4-[(4,6-dichloro-1,3,5-triazin- 2-yl) amino]-5-oxido-6-phenyldiazenyl-7-sulfonaphthalene-2-sulfonate	$C1_9H_{10}Cl_2N_6Na_2O_7S_2$	-	Affects activity of human proteins	Red crystalline powder	Wang et al., 2008)

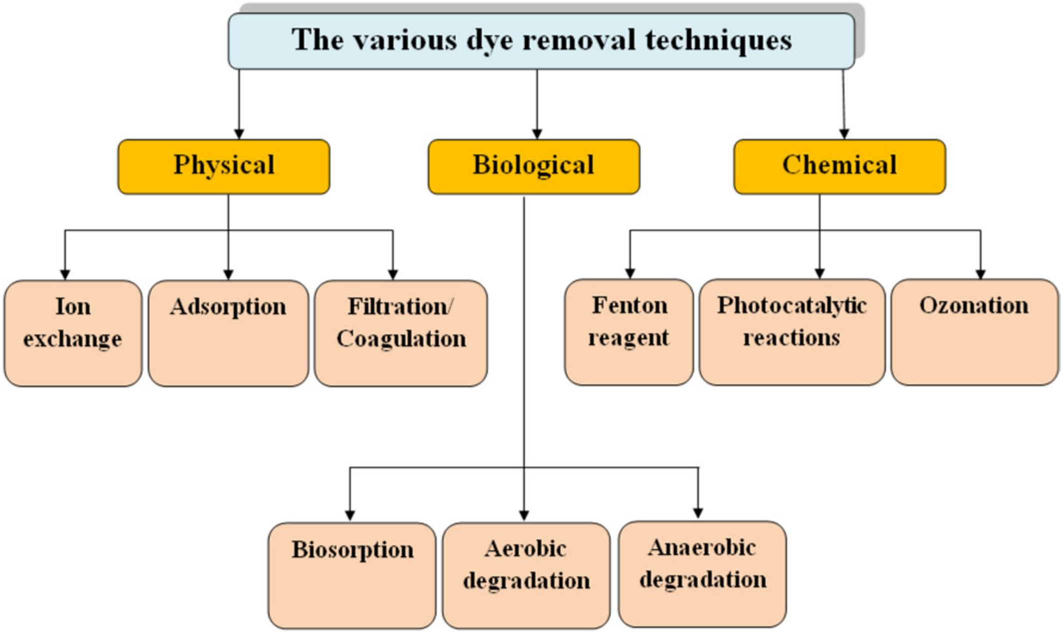

Fig. 5 Schematic representation of different dye removal techniques

and sonolysis. In real water matrices, energy requirements are strongly associated with the nature of contaminant. Regarding removal of a pollutant, a comparison table (Table 5) is presented depicting possible concentrations of water purification for above mentioned AOPs and total degradation percentages of heavy wastewater, such as leachates, and low-concentration pollutants such as antibiotics.

Tetracycline (TC), an antibiotic, is frequently provided to cattle feed and used to treat infections in both humans and animals. These applications are attributed to its inexpensive cost and broad spectrum of activity. Even in recent literature, TC has been referred as a potential COVID-19 treatment. The unfortunate fact is that only 25% of TC is metabolized by humans; remaining 75% is released into the environment. Residual TC has potential to adversely affect human health through biological food chain, impact the growth and development of aquatic flora and fauna, and cause endocrine disorders, mutagenicity, and antibiotic resistance. Therefore, it is crucial to figure out how to remove TC from water (Gopal et al., 2020; Lundström et al., 2016; Sodhi & Etminan, 2020).

Additionally, photo-Fenton is an important direction in photocatalytic technology. In particular, the photo-Fenton reaction can degrade dye wastewater efficiently and quickly.

C. Xiao et al. successfully synthesized novel Ni-doped FeOx catalyst through a simple co-precipitation method for simultaneous removal of Cr(VI) and various organic pollutants in heterogeneous photo-Fenton system. The removal efficiency of Cr (VI) and RhB still reached 90% and 91% in 10-NiFeO$_x$/H_2O_2/visible light system.

C. Xiao et al. successfully synthesized the burger-like α-Fe_2O_3 using $FeCl_3$ as iron source through a facile hydrothermal process. The α-Fe_2O_3 samples with spherical, elliptic, olive-like, and burger-like morphologies were obtained by adjusting hydrothermal reaction time, respectively. Under optimum operating conditions, degradation ratio of acid red G (ARG) by burger-like α-Fe_2O_3 reached 98% under visible light irradiation within 90 min (Xiao et al., 2018).

The kaolin–FeOOH catalyst was successfully prepared by C. Xiao et al. by using a facile method and exhibited excellent photo-Fenton catalytic performance with the assistance of oxalic acid. Benefiting from the high photosensitivity of iron–oxalate complexes of oxalic acid, 98.8% degradation percentage and 49.1% removal rate of

Table 2 Different physical dye removal methods with their benefits and drawbacks (Hethnawi et al., 2017; Holkar et al., 2016; Yagub et al., 2014)

Serial no	Techniques	Description	Advantages	Disadvantages
1	Irradiation	The elimination of dye molecules from dye effluent is done using radiation	Efficient at a lab scale	It costs a lot of money and takes a lot of dissolved oxygen
2	Adsorption	Adsorbents made from materials with high adsorption capacities are used to adsorb dye molecules	Reusable adsorbent. Best method of dye removal for a wide range of dyes	Adsorbents are very costly
3	Reverse osmosis	Deposited pollutants on one side and water on the other using a pressure-driven device in which water was forced across an extraordinarily thin membrane	Produces pure and clean water, is a common method for cycling water, and is efficient in removing various dye colors	Requirement of high pressure and very costly
4	Ion exchange	Ions from dye wastewater exchange with similar ions bound to a stationary solid surface in a reversible chemical reaction	Produce high quality of water, regenerable and good dye removal method	Effective only for few number of dyes
5	Membrane filtration	Dye particles are segregated after dye wastewater passes over a membrane	Efficient at recovering and reusing water	Unsuitable for dye removal, produces concentrated sludge
6	Nanofiltration and ultrafiltration	Dye particles are removed from clean water when wastewater is passed over a membrane with small pores	Effective for any type of dye	Short life span, requirement of high pressure, costly and high energy consumption

Table 3 Benefits and drawbacks of different chemical dye removal methods (Forgacs et al., 2004; Katheresan et al., 2018; Klein et al., 2015; Salleh et al., 2011; Vickers, 2017)

Serial no	Techniques	Description	Advantages	Disadvantages
1	Ozonation	In order to eliminate dye particles, ozone is produced from oxygen	Rapid response, gaseous consumption, and inability to expand the volume of wastewater	Unstable method, very costly and produce toxic by products
2	Fenton reaction	Using Fenton's reagent, dye particles can be removed from wastewater	It is excellent for dye wastewater with a solid content, gets rid of all the toxins in the water, and can remove both soluble and insoluble colors	Long reaction times, inability to remove dyes from vats, and limited pH range of operation
3	Oxidation	For the treatment of dye effluents oxidizing agents used due to which complex dye molecules breakdown into $CO_2$and H_2O	Short reaction time, can completely degrade dyes. Straightforward application	pH dependent, requirement of catalyst for efficient removal, costly
4	Photochemical	Wastewater is treated with the Fenton reaction and UV radiation to remove dye molecules	No sludge and foul odors production, effective dye removal method	Quite pricey and produces a lot of byproducts
5	Advanced oxidation process	Several oxidation processes are conducted simultaneously to get rid of dye particles	Can remove dye and hazardous compounds in rare circumstances	Production of undesirable by-products, not flexible and expensive
6	Ultraviolet irradiation	In wastewater, UV light is utilized to decompose dye particles	No sludge production	Limited treatment time, costly, energy depletion

TOC due to RhB degradation were achieved under optimum operating conditions (Chen et al., 2020).

Q. He et al. prepared a kaolin-Fe_2O_3 (K-Fe_2O_3) photocatalyst by a facile method. In a K-Fe_2O_3/PS/visible light system, a 99.8% degradation ratio of RhB was reached under optimal experimental conditions (He et al., 2020). $FeWO_4$ nanosheets as an example, the activation of oxalic acid (OA) based 13 on facet engineering for the enhanced generation of active radical species is reported, revealing 14 unprecedented surface Fenton activity for pollutant degradation. Density functional theory calculations confirmed more efficient generation of reactive oxygen species over $FeWO_4$ nanosheets with {001} facet exposed (FWO-001) under visible light irradiation compared to efficiency of $FeWO_4$ nanosheets with {010} facet exposed (FWO-010), which could be attributed to higher density of iron and efficient activation of OA on {001} facet (Li et al., 2019).

Advanced oxidation processes can also be divided into Fenton systems, represented by H_2O_2 (•OH), and systems, represented by peroxymonosulfate (PMS) and persulfate (PDS) ($SO_4^{\bullet-}$), based on various free radicals. The oxidative power of $SO_4^{\bullet-}$ was higher (2.5–3.1 V) and its half-life was longer (30–40 s) than those of •OH (1.8–2.7 V and 20 ns), making it more efficient at degrading aqueous pollutants (Huang et al., 2021a; Huo et al., 2020).

Researchers have paid increased attention to persulfate-based advanced oxidation processes (PS-AOPs) in recent years, largely as a result of increased prevalence of carbon materials and discovery of a non-radical pathway. Graphene (G), carbon nanotubes (CNTs), and biochar (BC) have all seen extensive application in persulfate-based advanced oxidation processes (PS-AOPs). H. Luo et al. demonstrated active locations of G, CNTs, BC, and other carbon materials, and generalized the methods for promoting carbon material activity and switching reaction pathways in PS-AOPs. Reactive oxygen species (ROS) and structures were discussed in context of functions of carbon materials in PS-AOPs. However, predominant ROS formation is linked to active sites on carbon materials, despite the fact that ROS are often complex in AOPs (Luo et al., 2022).

To further activate persulfate (PS) for tetracycline (TC) degradation, nitrogen and copper co-doped biochar (N-Cu/biochar) material was also studied. With a 200 mg/L catalyst concentration, 0.5 mM PS

Table 4 Different biological dye removal methods with their benefits and drawbacks (Adegoke & Bello, 2015; Manavi et al., 2017; Srinivasan & Viraraghavan, 2010)

Serial no	Techniques	Description	Advantages	Disadvantages
1	Enzyme degradation	To degrade dye molecules, extracted enzymes are used	Affordable, nontoxic, able to use enzymes to degrade dyes, and reusable	Production of enzymes is inconsistently high
2	Mixed and pure culture	Algae, bacteria, or fungi combined with the appropriate chemicals to remove dye	Reusable and effective for removing azo dyes	Sludge production results in harmful byproducts that need to be post-treated using traditional methods
3	Fungal culture	In order to grow, fungi break down dye molecules and consume them	Flexible approach that can simultaneously remove multiple dye types	Large reactors are necessary for full dye removal; unstable system
4	Algae degradation	For self-growth, algae ingest dye particles	Easy to assess, environmentally beneficial technique that can consume dyes	Unstable system
5	Microbial biomass-based adsorption	Various organic living organisms are combined to absorb dye particles	Several dyes exhibit an extraordinary affinity for microbial biomass	Not a reliable technique for all dyes
6	Aerobic-anaerobic combination	Complex dye molecules are broken down by a prepared sludge	Range of dyes can be fairly discolored; no foam formation	Requires a big land area, takes a long time, creates sludge, and does not entirely eliminate all dye particles

Table 5 Comparison of AOP degradation efficiencies in leachates and antibiotic effluents

AOP	Waste/contaminant	pH	Time (min)	Reaction condition	Waste degradation (%)
UV/H_2O_2	Ibuprofen	7	<30	11 W	60
Sonolysis	Ibuprofen	3	30	21 mg/L–300 mL, 300 kHz	98
Sonolysis	Diclofenac	5.3	180	16.6 g/L, 200 mL, 45 kHz	60
Sonolysis	Ibuprofen	n/a	180	14.6 g/L, 45 kHz	60
O_3/UV/H_2O_2	Enrofloxacin	11	20	1.4 L, 15 W	n/a
Sonolysis/Fenton	Diclofenac	n/a	40	20 mg/L, 20 kHz, 200 mL	73
Sonolysis/Fenton	Ibuprofen	2.6	120	20 mg/L, 862 kHz	100
Sonolysis/Fenton	Ibuprofen	2.6	120	20 mg/L, 20 kHz, 1 L	97
Sonolysis/Fenton	Ibuprofen	2.6	120	20 mg/L, 12 kHz, 1 L	95
Fenton	Ibuprofen	2.6	180	20 mg/L	80
UV/TiO_2/H_2O_2	Amoxicillin	5	30	600 mL, 6 W,100 mg/L	n/a
Sonolysis	Ibuprofen	4.3	180	20 mg/L, 862 kHz	80

concentration, and pH of 7.0, all TC was removed in 120 min. Bioluminescence inhibition assay was employed to figure out the toxicity of TC and its metabolites. The N-Cu/biochar/PS system, with its high catalytic efficiency and low consumables, could be a novel approach to wastewater remediation (Zhong et al., 2020).

The work by Y. Yuan, H. Luo, et al. provided new insight on the process of removing hexavalent chromium (Cr(VI)), which helped researchers to better define the scope of applications for sulfidated nanoscale zero-valent iron (S-nZVI) in Cr(VI) remediation (Yuan et al., 2022).

The removal of Cd(II) and Pb(II) from water was also studied by R. Huang and H. Luo et al. adopting three inexpensive adsorbents: pure raw attapulgite (A-ATP), high-temperature-calcined attapulgite (T-ATP), and hydrothermal loading of MgO (MgO-ATP). The goal of this research was to shed light on MgO-ATP and its potential as an economic and effective adsorbent for cleaning up polluted environments that have been contaminated with harmful metals like Cd(II) and Pb(II) (Huang et al., 2020).

Porous carbon nanomaterials have received a lot of attention recently as PMS activators (Hu et al., 2021). The oxidation of Fe0 can be slowed down by metal particles enclosed in hierarchical carbon layer of these materials. Additional favorable factors for PMS activation include carbon layer's tunable surface chemistry and their outstanding electron transport capabilities (Huang et al., 2021b, c). Having metal ions or clusters in the center and organic legends acting as a binding agent, metal organic frameworks (MOFs) are highly arranged porous materials (Ye et al., 2020). MOFs are extensively used in adsorption catalytic oxidation and other similar processes (Zhang et al., 2021, 2022a). Because of their large surface area and porosity, adjustable pore size, high conductivity, and stability, carbon compounds generated from MOF have recently received exhaustive study for the activation of PDS and PMS (Hao et al., 2021). Through straightforward pyrolysis of [Fe, Cu]-BDC precursor, Tang et al. effectively created a three-dimensional flower-like catalyst (i.e., FeCu@C) that contains iron-copper bimetallic NPs within a mesoporous carbon shell and was used to degrade sulfamethazine. Cu species facilitated quick Fe^{3+}/Fe^{2+} redox cycles, which increased •OH production (Tang & Wang, 2019). Since addition of FeNx sites regulates the electronic structure of catalysts, He et al. effectively synthesized carbon nanocubes containing a lot of FeN_x active sites by calcining xFe@ZIF-8. These electron-deficient Fe centers serve as electron acceptors to take in electrons that adsorbed PMS transmits, producing highly reactive $^1O_2$ for quick phenol oxidation. (He et al., 2021). In order to achieve degradation of phenol by activating PDS, Li et al. synthesized iron/carbon composites by pyrolyzing MIL-88A (Fe). During this process, optimized catalyst Fe_xC-600 performed superbly (Li et al., 2020). The advantage of carbon-coated metal nanoparticles is uniform distribution of metal particles throughout carbon layer, which is achieved by calcining MOFs at high temperatures in an Ar environment. Additionally, carbon encapsulation of metal particles can prevent them from aggregating (Liu et al., 2018).

4.1 SR-AOPs by MILs

Materials of Institute Lavoisier (MILs) are one of the typical representatives of MOF materials, which are synthesized by different transition metal elements (such as Fe^{2+}) and dicarboxylic acid ligands such as succinic acid and glutaric acid. Compared with metal oxides, MILs have unique advantages like porosity and unsaturated metal sites, which make them widely applicable in the field of catalysis. In sulfate radical advanced oxidation processes (SR-AOPs), coordinated unsaturated metal ions (CUS) mainly supplied by MILs can activate PMS/PS to form $SO_4^{\bullet -}$ and •OH, which have strong oxidizing properties and thus degrade organic pollutants in water. Also, MILs have a high specific surface area and pore volume, which not only provides high-density active centers and large reaction space, but also effectively adsorbs organic pollutants in water, thus facilitate the formation of $SO_4^{\bullet -}$, and •OH to react with organic substances(Huang et al., 2021c). Iron-containing MILs have been widely used in catalysis field. The richness, environmental friendliness, excellent magnetic separability and cost-effectiveness of Fe-based heterogeneous catalysts make them powerful candidates for SR-AOPs. Therefore, they have received particular attention in SR-AOPs. For example, (Li et al., 2016) synthesized four kinds of pure MILs including MIL-101(Fe), MIL-100(Fe), MIL 53(Fe), and MIL-88B(Fe) by simple solvothermal method. The azo dye acid orange 7 (AO7) degradation experiment showed that these MILs could accelerate PS activation to produce $SO_4^{\bullet -}$. The MIL-101(Fe)/PS system presented the best degradation efficiency, which indicated that catalytic capacity was closely related to the active sites of catalyst and different cage sizes.

4.2 Graphene-Based Materials

Graphene-based materials, which usually have good chemical durability and adsorption capacity, have been demonstrated as eco-friendly candidates for environmental catalysis. In previous studies, nanostructured graphene and graphene derivatives such as graphene oxide (GO) and reduced graphene oxide (rGO) was employed to activate PMS/PDS for degradation of target pollutant and graphene showed much poorer catalytic performance than GO and rGO. Although graphene has been employed as an adsorbent for various pollutants, its efficiency for the activation of persulfates is limited, which is ascribed to poor electron supply capacity by its stable π-conjugated system (Bekris et al., 2017). Pristine graphene oxide is also highly stable with poor reactivity due to the excess of oxygen content. In contrast, GO with relatively lower oxygen content has higher catalytic activity (Hu et al., 2017). GO requires surface modification, such as heteroatom doping and chemical/thermal reduction to rGO, to improve the catalytic activity. The reduction of GO will change the amounts and distributions of oxygen-containing functional groups on its surface, which influences catalytic activity and adsorption ability. It was found that adsorption ability was generally enhanced with increase of reduction degree of GO by introducing electron-donating functional groups, which benefited oxidation process occurred on rGO (Oh & Lim, 2018). Duan et al. found that rGO-900/PMS achieved complete removal of phenol in 150 min, and degradation efficiency was promoted when rGO synthesis temperature was elevated, due to removal of excessive oxygen groups (Duan et al., 2016). For degradation of various organic pollutants persulfates activation by carbon materials supported with metal has depicted in (Table 6).

In every AOP, production of free and strong OH radicals is achieved through different sources of power and materials. Firstly, in UV peroxide AOPs, power from UV radiation is capable of producing necessary OH radicals. In contrast to Fenton processes, addition of Fe^{3+}/Fe^{2+} ions with H_2O_2 (Fenton reagent) produces highly active Fe^{2+}/Fe^{3+} ions, respectively, with OH radicals providing the necessary catalytic system to properly treat specific wastewater. In electro-Fenton reactions, the process utilizes electrical energy to split the water molecule into OH free radicals with simultaneous presence of Fe ions. Ozone-based processes use photons (hν) to initiate the production of hydrogen peroxide which, in turn, produces OH radicals. In photocatalysis, a metaloxide catalyst is used, which utilizes the UV/

Table 6 Activated of persulfates by carbon materials supported with metal for degradation of organic pollutants

Catalysts	Catalysts dosage	Oxidant	Pollutant	Reaction condition	Degradation efficiency (%)
NiO-$NiFe_2O_4$-rGO	1.5 g/L	PMS	Rhodamine B	Pollutant concentration-20.16 mg/L pH-7.0 Time-40 min	100
TiO_2-GO	0.1 g/L	PDS	Diclofenac	Pollutant concentration-100 mg/L pH-5.54 Time-14 min	93.06
MnO_2-rGO	0.1 g/L	PMS	4-Nitrophenol	Pollutant concentration-50 mg/L pH-7.0 Time-30 min	100
$CoFe_2O_4$-GO	0.2 g/L	PMS	Rhodamine B	Pollutant concentration-0.03 mM pH-7.0 Time-12 min	100
CuO-rGO	0.1 g/L	PDS	2,4,6-Trichlorophenol	Pollutant concentration-0.1 mM pH-6.0 Time-180 min	100
Fe_3O_4-Mn_3O_4-rGO	100 mg/L	PMS	Methylene Blue	Pollutant concentration-50 mg/L pH-7.0 Time-30 min	98.8
Fe_3O_4-AC	0.2 g/L	PDS	Tetracycline	Pollutant concentration-20 mg/L pH-5.5 Time-180 min	99.8
γ-MnO_2-$ZnFe_2O_4$-rGO	0.2 g/L	PMS	Phenol	Pollutant concentration-20 mg/L pH-7.0 Time-30 min	100
$CoFe_2O_4$-GO	0.3 g/L	PMS	Norfloxacin	pH-7.0 Time-20 min	100
Co_3O_4-graphene	0.05 g/L	PMS	Orange II	Pollutant concentration-0.03 mM pH-7.0 Time-10 min	100

Vis radiation to create electron hole pairs for the generation of OH free radicals. Ultimately, energy from ultrasound (sonolysis) is efficient for rapid production of H and OH radicals with high yield. In Table 7, the main advantages and disadvantages of each AOP are presented.

5 Photocatalysis

The majority of fluorine-containing wastes are currently dumped in landfills or used for low-value purposes; thus, it is necessary to carry out high value-added resource treatment for slag utilization. Industrial effluents, such as colorless antibiotics and colored dyes, have recently risen to forefront of concern due to their widespread distribution in water bodies, which threatens the natural system. The decomposition of organic pollutants using photocatalytic technology is proven to be successful and promising.

Under the influence of ultraviolet (UV) or visible light, a catalyst is used to speed up chemical reactions in a photocatalyst. The words “photo” and “catalysis” come from ancient Greek. Light is the “photo” in “photocatalysis,” which increases the rate of a reaction using an exogenous material (the “catalyst”) that is not itself consumed in the process. A catalyst minimizes activation energy required for a chemical reaction, boosting the rate of reaction. To sum up, photocatalysis is the technique of using light and catalysts to speed up a chemical reaction. Photocatalysis can be either homogeneous or heterogeneous, depending on the photocatalysts used (Esplugas et al., 2007).

Table7 Advantages and disadvantages of AOPs

AOP	Advantages	Disadvantages
Fenton-based	• Exploitation of Fe ions and UV/voltage • The versatility of Fe ions to react with pollutants • Highly active in acidic pH conditions	• Slow reaction rate • Metal-containing sludge byproducts • Fenton reagent preparation cost • Chlorate formation in alkaline solution
Ozone-based	• High reaction rate (high production of •OH due to O_3 splitting) • More stable byproducts • Effective in pretreatment for water purification	• Formation of genotoxic compounds • Low solubility in water/drawbacks in aqueous reactions • Self-decomposition
Sonolysis	• Higher •OH production • Lack of reagents	• Parameter versatility • Uncontrolled byproducts • Targets low-concentration wastewater
Photocatalysis	• Stability, low-cost, nontoxicity • Effective due to catalyst surface in water pollutant degradation • Environmentally friendly/low pollutant load of byproducts	• Improper catalyst selection • Radiation wavelengths require high operational costs

To degrade the pollutant dyes, heterogeneous photocatalysis includes a number of reactions. However, homogeneous photocatalysis includes metal complexes as a catalyst. In recent years to degrade harmful dyes, excellent heterogeneous photocatalysts are wide band gap semiconductors such as ZrO_2, TiO_2, SnO_2, CeO_2, ZrO, ZnO, etc. Band gap of certain metal oxides is given in Fig. 6. Production of electron–hole pairs on the illumination of light is materials properties as a photocatalyst. The recombination time of electron–hole pair is higher for a decent photocatalyst. Further, these e^-/h^+ pairs produce hydroxyl radicals (OH) and superoxide radicals (O_2^-) which have been demonstrated as excellent scavengers for photocatalytic degradation of harmful dyes.

5.1 Basic Mechanism of Photocatalysis

Band gap energy (E_g) is difference of energy between the top of valence band (VB) and the bottom of conduction band (CB). If energy of light (which is illuminating on the solution of catalyst and organic dye) is higher than band gap of catalyst, excitation of e^- will takes from VB due to which generation of h^+ occurs in VB. These electrons and holes will migrate to catalyst's surface. The e^- form superoxide radicals ($O_2^{\bullet -}$) upon reacting with O_2 available from surroundings and holes h^+ form hydroxyl radicals ($OH^{\bullet}$) on reacting with water in the solution. During photocatalytic oxidation, these radicals react with organic dyes in order to get H_2O and CO_2 as final products (Rehman et al., 2009). Basic photocatalytic mechanism is shown by Fig. 7 and can also be understood with the help of given reactions (Suman et al., 2021a):

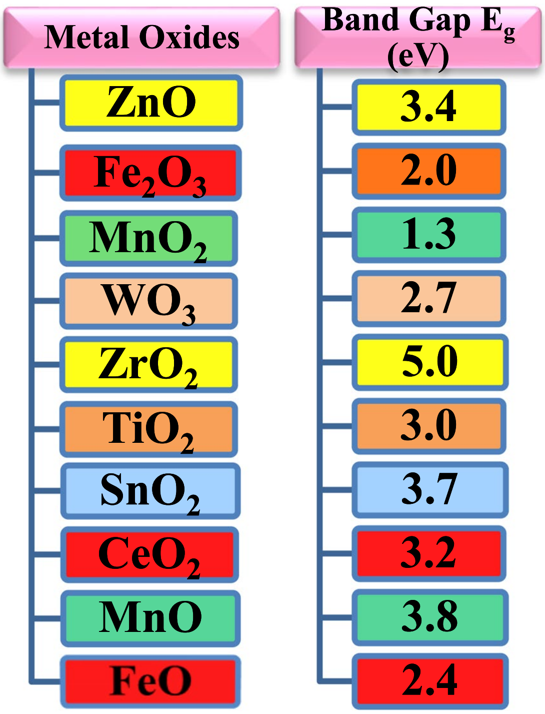

Metal Oxides	Band Gap E_g (eV)
ZnO	3.4
Fe_2O_3	2.0
MnO_2	1.3
WO_3	2.7
ZrO_2	5.0
TiO_2	3.0
SnO_2	3.7
CeO_2	3.2
MnO	3.8
FeO	2.4

Fig. 6 Various semiconducting metal oxides with their band gap

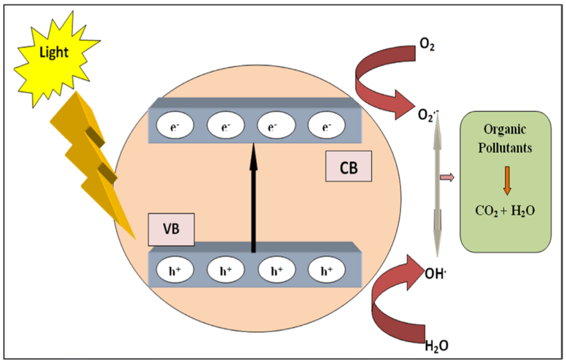

Fig. 7 Systematic mechanism for photocatalytic degradation of pollutants by semiconducting metal oxides

$$H_2O + h^+ \rightarrow OH^- + H^+$$

$$e^-_{CB} + O_2 \rightarrow O_2^{\bullet -}$$

$$h^+_{VB} + OH^- \rightarrow OH^{\bullet -}$$

$$Dye + O_2^{\bullet -} + OH^{\bullet} \rightarrow H_2O + CO_2$$

The following benefits make photocatalysis best technology for treating wastewater:

- Photocatalysis produces non-hazardous byproducts, which is a major advantage.
- Complete mineralization of organic dyes.
- The band gap of photocatalytic material determines whether or not ultraviolet (UV) light can be used instead of sunlight.
- Dye degradation can make use of the environment's plentiful oxygen supply.
- For photocatalysis, scientists turn to semiconductor metal oxide photocatalysts since they're cost effective, stable chemically, recyclable, and non-toxic.
- Photocatalysis is a cost-effective and eco-friendly strategy for dye degradation.

5.2 Metal Oxide Nanoparticles as Photocatalysts

Metal oxides are crystalline solids consisting of an oxide anion and a metal cation. Normally, they interact with acids to produce salts and with water to produce bases. These nanoparticles possess exclusive optical properties like UV absorption, dichoism, specific color absorption in visible range of spectrum, photoluminescence, etc. Also, these nanoparticles have unique physical and chemical properties which are ascribed to large density and small size of edges as well as corners on their surface. Since particle dimension/size is small at nanoscale, a significant portion of atoms would be on the surface of particles. The reactivity of nanoparticles increases as the effective surface area increases because they are capable to react to a larger extent in comparison to that of normal crystals. Consequently, there are many metal oxide nanoparticles on the surface in order to react with incoming molecules. In metal oxide nanoparticles specifically like ZnO, CeO_2,SnO_2, TiO_2, CuO, ZrO_2, etc., stress or strain and adjoining structural perturbation are generated by increasing number of interface and surface atoms as size decreases in case of nanoparticles (Hosseini et al., 2022). In comparison to reactivity of bulk, metal oxide nanocrystals exhibit intrinsically greater chemical reactivity due to their unique surface chemistry (Naseem & Durrani, 2021).

Due to size-related structural alterations, changes in cell parameters have been observed in nanoparticles of SnO_2, TiO_2, CeO_2, ZnO, ZrO, AgO, MgO, CuO, etc. Due to their small size and significant surface area, metal oxide nanoparticles exhibit exceptional catalytic properties. For ecological remediation, particularly in the decomposition of organic pollutants present in wastewater, photocatalytic active materials dependent on nanomaterials of metal oxides are frontliners. These nanoparticles are well-suited for photocatalytic oxidation and removal of organic pollutants ion because to their superior surface, structural, and crystalline features (Ahmed & Mohamed, 2022). Hence, metal oxide nanomaterials like TiO_2, CeO_2, SnO_2, ZrO_2, MnO_2, WO_3, Cu_2O, CuO, and ZnO focusing on photocatalytic applications have outstanding performances (Park et al., 2022; Rajendiran et al., 2022).

The structural design, size, and shape of nanostructures have a significant impact on aforementioned properties of metal oxide nanoparticles. Consequently, structural characteristics and fundamental properties of functional devices are affected by number of factors which in turn have influence on their performance. For the manufacture of metal oxide nanoparticles with tunable structural features and properties, a sustainable and acceptable technique should include optimization of all process parameters that could result in unfavorable adjustment of obtained characteristics (Theerthagiri et al., 2018).

5.3 Photocatalytic Performance of MONPs and Effect of Rare-Earth Doping

Initially photocatalysis mechanism requires retainment of light irradiation higher in comparison to threshold band gap energy, which is a property of semiconducting materials. Absorption of light quantum results in photogeneration of e^- and h^+ in CB and valence band VB, respectively. These electron–hole pairs degrade organic pollutants upon reacting with them by diffusing on surface of metal oxides during photocatalytic degradation reaction. Metal oxides have emerged as most important photocatalysts for environmental rehabilitation of polluted drinking water and industrial wastewater over past few decades. Many semiconducting photocatalysts, including WO_3, ZrO_2, SnO_2, CeO_2, Cu_2O, and others, have been used because of their superior optical, electronic, and anisotropic properties, such as high surface area, environmental friendliness, efficiency, cost, toxicity, availability, stability, and resistance to different irradiation wavelengths.

Although, most of metal oxides show good photocatalytic properties but TiO_2 has gained much importance towards photocatalytic activity because of its outstanding electrical, optical properties and chemical stability. TiO_2 nanoparticles have three crystalline phases: (1) rutile, (2) anatase, and (3) brookite. Out of all three phases, anatase is highly efficient and stable in photocatalytic degradation of organic pollutants due to its open structure in comparison to that of rutile phase. Among rutile and brookite phases, photocatalytic activity is also shown by rutile phase but to a smaller extent; however, no appreciable photocatalytic activity is displayed by brookite phase.

Charge transfer properties, favorable combination of electronic structure and lifetime of exciton (MONPs) has made it feasible for their utilization in the field of photocatalysis. Although MONPs have various useful properties but there are also some disadvantages for certain photocatalysts which prohibit their large-scale applicability in the field of photocatalysis. Broad band gap (3.2 to 3.4 eV) of metal oxides (ZnO, TiO_2 etc.) limits their photocatalytic activities to ultraviolet (UV) region of light. Besides of it, narrow band gap (2.6–3.0 eV) of metal oxides like CuO, V_2O_5, WO_3, Fe_2O_3 etc. have the capability to retain maximum solar light which is responsible for hasty recombination of e^-/h^+ pairs which in turn decreases charge kinetics process and eventually overcome photocatalytic activity of semiconducting metal oxides. Consequently, there is a solid need to plan and use effective metal oxide photocatalytic materials with better properties to overcome these drawbacks. Doping of rare earth elements like La, Ce, Er, Gd, Yb, Sm etc. is vastly employed strategy for enhancement of photocatalytic performance of metal oxide nanoparticles (MONPs). Modification of metal oxides can be done by creating point defects like oxygen vacancies, doping impurities and metal interstitials (Buelens et al., 2019; Raizada et al., 2021; Yuan et al., 2016). It has been investigated by many researchers that rare earth doping improves the photocatalytic, surface and optical properties of metal oxides. Rare earth doping has also been shown to shift the working wavelength, which in turn shrinks band gap to visible region of the spectrum. Thus, narrowing of band gap improves MONPs' photocatalytic performance. Rare-earth doping also leads to formation of oxygen vacancies as defects, which are responsible for increasing degradation efficiency because their presence and character lower the band gap and shift the oxide's response towards visible spectrum (Zhang et al., 2022b).

As a result of the doping with rare earth elements, the following occurs:

1. Enhancement in photocatalytic activity
2. Visible light absorption increases
3. Active surface area increases
4. Enhancement in thermal stability
5. Band gap decreases
6. Effectual separation of photogenerated e^-/h^+ pairs

To observe the photocatalytic effectiveness of La doped CeO_2 for degradation of Rose Bengal (RB) dye, photocatalytic test was performed. The absorption curves at various time durations under exposure of UV light for RB dye solution are shown in Fig. 8.

Degradation of dye is shown by regular decrement in intensity of peak. It has been found that degradation percentage enhances from 76.7 to 86.7% for 2% La-doping to 8% La-doping. Figure 9a depicts decrement in relative concentration of dye with exposure time. Figure 9b depicts percentage degradation efficiency versus. Linear fitting of –ln (C/Co) with respect to time is shown in Fig. 9c and variation in electricity cost with dopant (La) content is calculated in Fig. 9d.

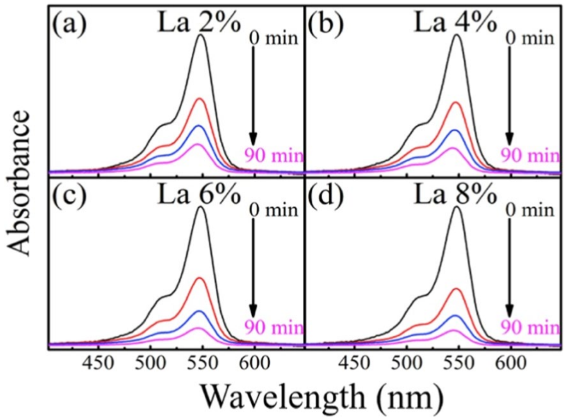

Fig. 8 Using doped CeO_2 nanoparticles (La 2%, La 4%, La 6%, and La 8%) as a catalyst, absorption spectrum of dye under exposure of UV light at various time intervals, Adapted from S. Chahal et al. (Chahal et al., 2020a) with License number 5291141157730

Comparative study of cerium (Ce), lanthanum (La), and neodymium (Nd) doped SnO_2 was observed for photodegradation of phenol in aqueous solution. Figure 10a shows the relative concentration of dye versus time for La-doped SnO_2. Degradation efficiency continuously increases with increment in Ce-doping in host lattice as displayed by Fig. 10b. Figure 10c depicts relative dye concentration versus time for Nd-doped SnO_2. Upon utilizing 0.4 wt% Ce: SnO_2 catalyst, 86% phenol was found to be degraded after 120 min. of irradiation time. It has also been observed that the photocatalytic performance increases from 57% (0.2 wt% Nd: SnO_2) to 95% using 0.6 wt% Nd: SnO_2 as a catalyst. However, only 24% of phenol has been found to be eliminated upon using undoped SnO_2 catalyst under same irradiation time. 100% degradation of phenol was observed for 0.6% La: SnO_2 catalyst. Figure 15 presents comparison of decrement in the concentration of phenol dye with the help of different rare-earth (La, Ce, Nd) doping SnO_2 nanoparticles. Hence, it can be concluded that amongst three dopants, La-doped-SnO_2 samples are highly photoactive as 100% phenol was degraded under equivalent exposure time.

Fig. 9 **a** Variation in C/C_O with degradation time, **b** degradation % of dye with respect to exposure time, **c** linear fit of exposure time and -ln (C/Co), and **d** electricity cost for La 2%, La 4%, La 6%, and La 8% doped CeO2 nanoparticles. Adapted from S. Chahal et al. (Chahal et al., 2020a) with license number 5291141157730

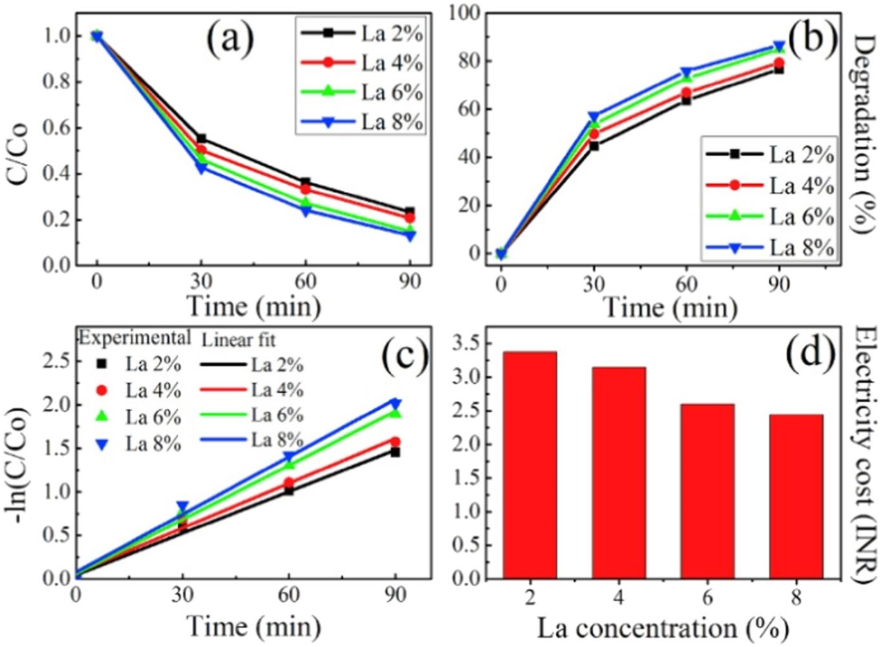

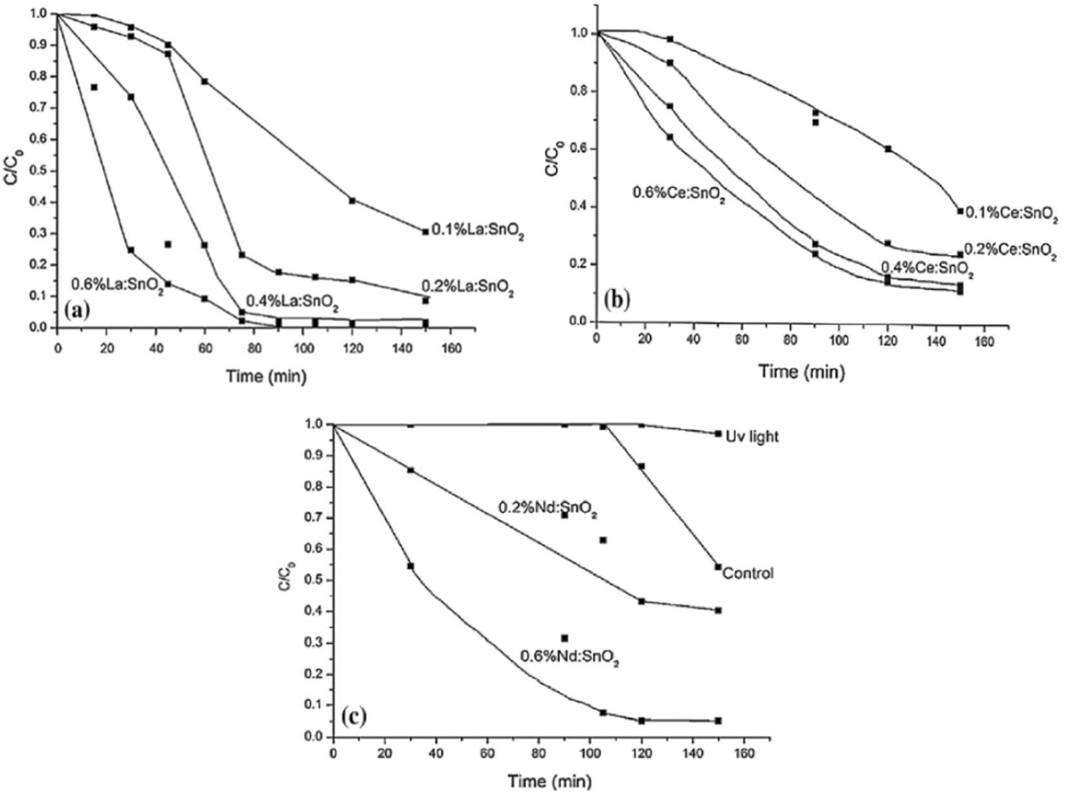

Fig. 10 Comparison of decrement in the concentration of phenol with multiple doping materials, **a** La-doped SnO_2, **b** Ce-doped-SnO_2, and **c** Nd-doped-SnO_2, under irradiation of ultraviolet light is shown in above graphs (Al-Hamdi et al., 2014)

The photocatalytic degradation efficiency of pristine ZnO, gadolinium (Gd)-doped ZnO, La-doped ZnO, and Gd/La co-doped ZnO nanoparticles was observed for degradation RhB dye and colorless pollutant tetracyanonickelate (TCN) under irradiation of sunlight as depicted in Fig. 11. In comparison to pristine ZnO photocatalysts, La/Gd co-doped ZnO showed greater degradation percentage. After 100 min of light irradiation, greatest RhB degradation efficiency of Gd/La@ZnO nanoflower was 91%, reflected in Fig. 11a. The dye degradation percentage for ZnO, Gd@ZnO, and La@ZnO was calculated to be 20%, 42%, and 26%, respectively. Using pseudo-1st-order kinetics, rate constant (k) for RhB degradation reaction was estimated, as shown in Fig. 11b Gd/La@ZnO photocatalyst has a k value of 0.023 min^{-1}, which is 4.6 and 7.7 times greater than Gd@ZnO and La@ZnO photocatalysts, respectively. In addition, photocatalytic effectiveness and kinetic plot of a colorless pollutant (TCN) was examined, as depicted in Fig. 11c, d. Gd/La@ZNO had a maximum degrading efficiency of 74% and a “k” of 0.013 min^{-1}.

The degradation of RhB dye under visible light illumination has been employed to test photocatalytic performance of pristine and Ce@WO_3nanorod samples (see Fig. 12a). Under illumination of visible light, blank experiment exhibit negligible degradation. Within 30 min, 11.5%, 23.3%, and 24% of dye were absorbed by tungsten oxide (WO_3), 3% Ce@WO_3 and 5% Ce@WO_3 before light on. The degrading efficiency of catalyst 3% Ce@WO_3 was observed to be 96%, which is 1.28 times higher than pure WO_3. The rate of photocatalytic degradation of RhB dye is shown in Fig. 12b. Notably, 3% ce@WO_3 catalyst has a higher K value (0.0318447 min^{-1}) than pure WO_3, which is 2.6 times greater. Figure 12c depicts the 3% Ce@WO_3 catalyst’s cyclic RhB dye degradation performance. The efficiency decreases from 90 to

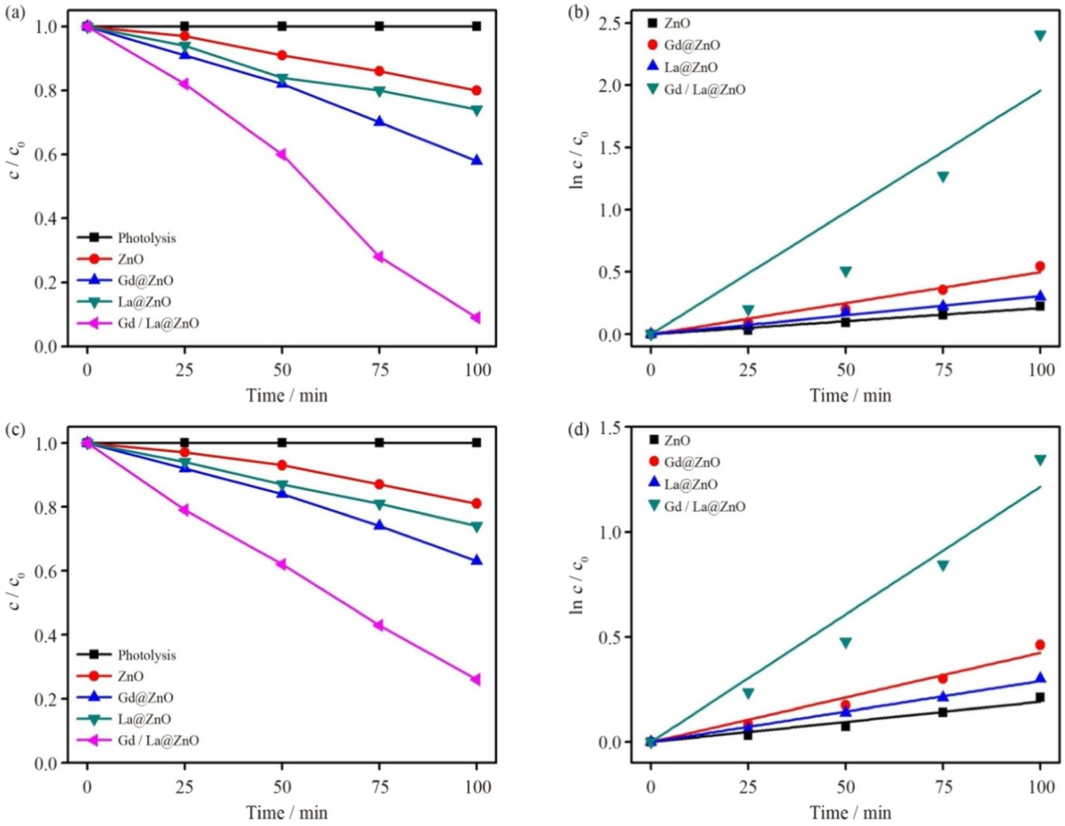

Fig. 11 **a** RhB dye degradation graph, **b** kinetic plot for RhB, **c** degradation plot for TCN dye, **d** kinetic plot for TCN. Adapted from B. Palanivel et al. (Palanivel et al., 2022) with license no. 5330261361587

89% when third cycle is completed. It demonstrates that 3% Ce@WO_3 nanorods is a fantastic photocatalyst. After the recycling test, XRD profile was collected, as shown in Fig. 12d. The catalyst's XRD pattern has not changed significantly. Thus, it examined the catalyst's enhanced photostability and reusability.

The photocatalytic activities of pure and rare earth (RE) ions (Ce, Eu) doped TiO_2 nanowires were investigated using degradation (C_0/C) of organic TBO dye in an aqueous solution shown in Fig. 13. Where, Co and C are the starting concentration and concentration of organic dye in reaction solution at time (*t*), respectively. Ce^{3+}:TiO_2 and Eu^{3+}:TiO_2 nanowire arrays, when exposed to UV light, degrade almost 90% of toluidine blue O (TBO) within 80 and 120 min, respectively. High surface area with large aspect ratio is strongly related to improvement in photocatalytic performance for RE-doped TiO_2 thin films (Bandi et al., 2013).

The impact of dopant concentration on photocatalytic performance of Gd-doped TiO_2 is shown in Fig. 14. The efficiency of MB decomposition rises initially and then falls when Gd doping content rises. When Gd content is 5 wt%, degradation percentage of MB reaches 90% in visible light with a wavelength of 405 nm, whereas pristine TiO_2 only reaches 76% after 10 min. This finding suggests that a small quantity of Gd doping can boost TiO_2's photocatalytic effectiveness (Tang et al., 2022).

The decrease in Congo Red (CR) concentration vs time for ZS (ZnO:Sm) sample is displayed in Fig. 15a, starting from varied values of initial dye concentration. Furthermore, Fig. 15b shows relationship between initial reaction rate (r_0) and apparent initial dye concentration (C_0) for ZS (ZnO:Sm) material. Finally, process optimization was done empirically using gradient approach. The optimal parameters for CR dye degradation in

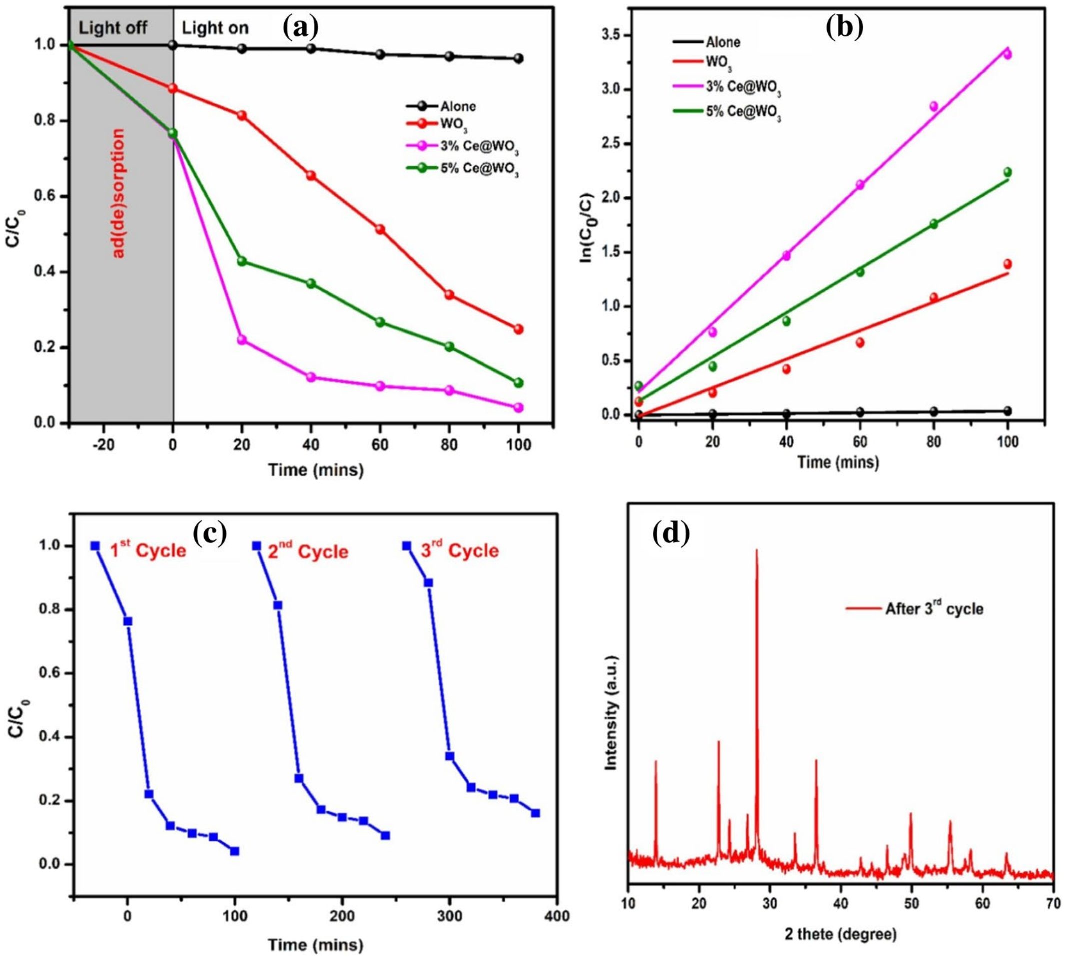

Fig. 12 **a** RhB dye degradation curve after photocatalysis. **b** Curve for pseudo-first-order kinetics, **c** Photocatalytic cycling test. **d** XRD patterns after completing third cyclic tests. Adapted from T.Govindaraj et al. (Govindaraj et al., 2021) with license no. 5330360878173

presence of ZS sample were found to be an initial dye concentration of 10.7 mg/L and a catalyst dose of 0.236 g/L. In these settings, a maximum color removal performance of 95.8% was measured experimentally. Thermal activation also allowed for successful recovery of wasted catalyst (Pascariu et al., 2019). How much rare earth doped metal oxides are efficient for water remediation are illustrated in Table 8.

5.4 Photocatalytic Performance of MONPs Doped with Transition Metal Ions

To improve photocatalytic performance of these wide band gap semiconducting metal oxide nanoparticles, use of transition metals as dopants, such as vanadium (V), tungsten (W), iron (Fe), cupper (Cu), silver (Ag), niobium (Nb), manganese (Mn), and so on, appears as a promising strategy (Chahal et al., 2022). A detailed literature survey of photocatalytic performance of transition metal ion doped MONPs are given in Table 9.

5.5 Photocatalytic Performance of Metal Oxide Nanocomposites

High photocatalytic efficiency is achieved by improving optoelectronic properties of photocatalysts, which in turn improves their light absorption, photo-induced charge separation, and charge transfer. As

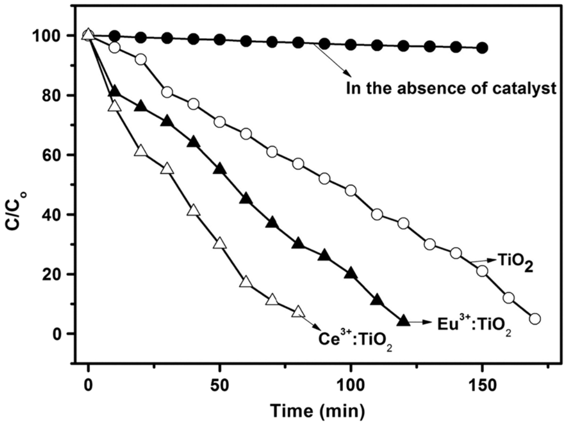

Fig. 13 In the lack and existence of pure and RE doped TiO_2 nanowire arrays, photocatalytic degradation (C/Co) of a TBO dye under UV irradiation. Adapted from V. R. Bandi et al. with license number 5333720375856

it has been already discussed that semiconducting metal oxides have shown great promise in the field of photocatalysis. Unfortunately, high recombination rates of these photogenerated e^- and h^+ pairs make these materials inefficient for photocatalytic activities (Suman et al., 2021b). In addition, wide band gaps of these materials also hinders their practical application in visible-light region of solar energy, which is the greatest source of energy on earth and sufficiently available. Moreover, when the surfaces of these nanomaterials are covered with products of catalysis reactions, interactions between incoming target molecules and surface are restricted by some extent. As a result, photoexcited e^- and h^+ pairs cannot be transferred for further photocatalytic reactions. Therefore, it has been realized that designing multi-component systems by assembling functional nanomaterials with metal oxide photocatalysts would be a better way to solve these issues (Rani et al., 2020; Suman et al., 2021c). Many metal oxide-based photocatalysts have been functionalized to boost their photocatalytic activity and electrical/optical features in response to these difficult problems. The fictionalization of metal oxide photocatalyst nanomaterials by coupling with transition metal oxides, ferrites or graphene nanostructures has attracted considerable interest in the development of high-performance photocatalytic systems in recent years. These multi-component nanocomposite systems composed of metal oxides, graphene (or its derivatives) and other metal oxides are highly significant as alternatives to extensively studied bi-component systems for the design of high-performance photocatalytic systems. The outstanding electrical and surface plasmon resonance capabilities of these nanomaterials make coupling of metal oxides with graphene and metals advantageous for the enhancement of optoelectronic features (Chahal et al., 2023).

Under influence of visible light, vanadium oxide (V_2O_5) nanorods operate effectively as photocatalysts. However, within 210 min of exposure time, 66.85% photodegradation was noted due to recombination of photogenerated electron–hole. In comparison to UV and Visible light, photocatalytic performance of

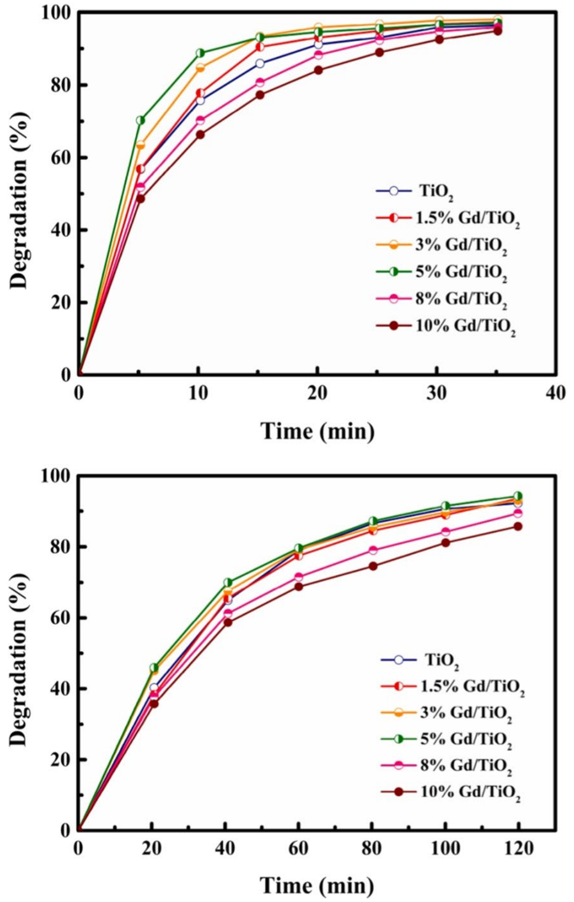

Fig. 14 Curves for the photocatalytic degradation of MB: **a** visible light; **b** all-weather simulated sunlight. Adapted from X. Tang et al. with license number 5333751076876

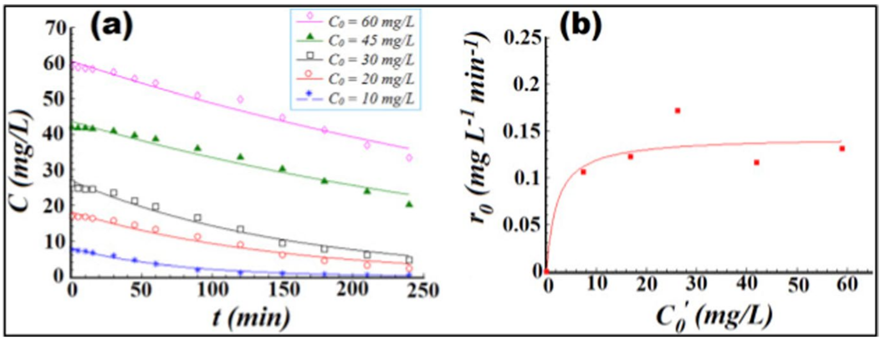

Fig. 15 **a** CR dye concentration decay as a function of reaction time (photo-catalytic reaction kinetics). **b** In existence of ZS (ZnO:Sm) material at various starting dye concentrations, correlation between the initial degradation reaction rate (r_0) and apparent initial dye concentration. Adapted from P. Pascariu et al. with license number 5333770757735

as-prepared grapheme oxide-vanadium oxide (GO-V_2O_5) nanocomposite was better under direct sunlight. The GO-V_2O_5 nanocomposite demonstrated nearly complete degradation of 97.95% of VB dye in 90 min under direct sunlight; however, degradation of VB dye under visible (96.93%) and UV light (78.35%) sources takes 180 and 210 min, respectively. Due to its effective charge transfer capabilities, which inhibit recombination of electron–hole pairs, as-synthesized GO-V_2O_5 nanocomposite exhibited greater photocatalytic activity compared to pure V_2O_5 (Beaula Ruby Kamalam et al., 2021).

Malachite green (MG) and methylene blue (MB) photocatalytic degradation with TiO_2 and rGO-Fe_3O_4/TiO_2 were observed under illumination of visible light by glancing at major absorption peak at 617 nm and 658 nm, respectively, as shown in Fig. 16a and b. The findings showed that rGO-Fe_3O_4/TiO_2 has a photocatalytic efficiency of 99% for MG and 97% for MB as compared to TiO_2, which has a photocatalytic efficiency of MG (67%) and MB (62%), respectively. Increased photocatalytic performance of rGO-Fe_3O_4/TiO_2 is correlated with the presence of reduced graphene oxide (rGO), which is significant for photocatalytic decomposition of MG (Bibi et al., 2021).

Figure 17 illustrates photo-Fenton performance of various samples (ZnO, Fe_3O_4, Fe_3O_4/GO, ZnO-Fe_3O_4/rGO) toward MB dye degradation. ZnO-Fe_3O_4/rGO nanocomposite sample needed 150 min to remove 97% of MB dye from an aqueous solution when exposed to visible light, whereas Fe_3O_4/GO could only decompose approximately 45% of total MB concentration. The electrons in VB of ZnO can thus be stimulated into CB of ZnO when exposed to visible light in ZnO-Fe_3O_4/rGO system, and they can then be successfully transferred to Fe^{3+}/Fe^{2+}redox pair in Fe_3O_4 across the graphene interlayer (Ojha et al., 2017). Table 10 lists various nanocomposites of metal oxides that serve as photocatalysts.

5.6 Nanostructured Metal Oxide Core–Shells and Their Photocatalytic Activity

5.6.1 *Mechanism for Photocatalysis in Core–Shell Nanostructures*

By using a schematic illustration such as shown in Fig. 18, it is possible to understand how electrons and holes move between shell and the core and how it affects photocatalytic performance. The •OH and O_2 radicals play a crucial part in decomposition of dye, contributing in transformation of hazardous dye molecules into non-toxic product. Excitation of VB and CB of core and shell during photodegradation process can result in generation of electrons and holes. A shift of energetic electrons from shell's CB to core's CB and a transfer of holes from shell's VB to core's VB can both occur during the core–shell interface. The hole that moved onto the surface of the shell improved the core's photostability. This prevents the recombination of photogenerated electron and hole. Superoxide ($O_2^{\cdot -}$) and hydroxyl (OH•)

Table 8 List of doped metal oxide nanoparticles that are UV/Visible light active having various dimensions and shapes along with their synthesis technique, morphology, and optical properties of particles for photocatalytic applications

Dimension	Morphology	Parent metal oxide	Dopant	Synthesis method	Characteristics of the obtained product	Pollutant	Degradation rate	Reaction condition	Ref
3D	Nanospheres	SnO_2	Ce	Hydrothermal	Ce-doped SnO_2 hollow spheres have diameter about 200–350 nm E_g: 3.5–2.6 eV	MG	92% degradation rate of MG dye was achieved in 120 min. under UV light irradiation	Catalyst dose–10 mg/L 500 W Hg lamp (intensity = 86 mW/cm^2)	Chen et al., 2021)
0D	Nanoparticles	SnO_2	Ce	Co-precipitation	The average crystallite size was observed to be 29.3–24.7 nm E_g: 3.4–3.1 eV	MO	94.5% degradation rate of MO dye was obtained in 100 min under UV/Vis light	Initial concentration–20 mg/L Catalyst dose–10 mg/L High-pressure mercury lamp (300 W)	Ali Baig et al., 2021)
1D	Nanorods	SnO_2	-	Hydrothermal	Average crystallite size lies between 110 and 120 nm Red shift	MB	SnO_2 hierarchical nanorods illustrate highest rate of degradation in comparison to pure SnO_2 under illumination of direct natural sunlight	Catalyst dose–50 mg/100 mL	Perumal et al., 2022)
0D	Nanoparticles	WO_3	Gd	Hydrothermal	Particle size was found to be 12 nm Red shift	MB	In 90 min, 98% of the MB dye was degraded	Initial concentration–20 mg/L Catalyst dose–0.02 g/100 mL Metal halide lamp (visible illumination) (400 W) 400 nm	Bilal Tahir & Sagir, 2019)
1D	Nanorods	ZnO	Nd, Gd	Hydrothermal	Average crystallite size was found to be 5.51–23.66 nm E_g: 3.31–2.88 eV	MB	93% degradation of MB dye in 120 min	Initial concentration–20 mg/L Catalyst dose–100 mg/L Tungsten lamp (300 W)	Akhtar et al., 2020)

Table 8 (continued)

Dimension	Morphology	Parent metal oxide	Dopant	Synthesis method	Characteristics of the obtained product	Pollutant	Degradation rate	Reaction condition	Ref
0D	Nanoparticles	CeO_2	Y	Sol–gel	Average crystallite size was found to be 9.8–9.1 eV E_g: 3.40–3.12 eV	RB	98% degradation of RB dye in 90 min under illumination of UV light	Initial concentration–5 mg/L Catalyst dose–50 mg/50 mL UV source of 300 W	Chahal et al., 2019)
0D	Nanoparticles	CeO_2	Sm	Sol–gel	Average crystallite was found to be 8.5–8.3 E_g: 3.23–3.17 eV	RB	Under UV light exposure, RB dye degraded about 89.04% in 90 min	Initial concentration–5 mg/L Catalyst dose–50 mg/50 mL UV source of 300 W	Chahal et al., 2020b)
0D	Nanospheres	TiO_2	Nd	Sol–gel	Particle size for Nd doped TiO_2 was found to be 4.2–5.6 nm E_g: 3.20–3.10 eV	Orange II	Nd doped TiO_2 shows best photocatalytic activity towards orang II dye compared to other rare earth	0.01 M Orange II dye 0.02 florescent lamp wavelength with power 8 W (254 nm)	Štengl et al., 2009)
1D	Nanoparticles	ZnO	La, Er, Sm	Electro spinning	Average crystallite size for pure and Sm, Er, La doped ZnO was found to be 33.7, 28.8, 22.7 and 30 nm Red shift	Congo Red	95.8% degradation of Congo Red dye was observed for Sm doped ZnO in 240 min under UV light	Initial concentration–30 mg/L Catalyst dose–0.1 g/600 mL Mercury lamp (150 W)	Pascariu et al., 2019)
0D	Nanoparticles	ZnO	Eu	Co-precipitation	Average crystallite for Eu doped ZnO was found to be 5.67 nm E_g: 3.28–3.31 eV	MO	95.3% degradation of MO dye was observed in 180 min under UV exposure	Initial concentration–10 mg/L Catalyst dose–0.1 g/100 mL High-pressure mercury lamp (100 W)	Zong et al., 2014)

Table 8 (continued)

Dimension	Morphology	Parent metal oxide	Dopant	Synthesis method	Characteristics of the obtained product	Pollutant	Degradation rate	Reaction condition	Ref
0D	Nanoparticles	ZnO	Cu	Sol–gel	Average crystallite size was estimated to be 32 nm and 28.5 nm Red shift	MO	Under UV light, MO dye degrades 88% after 4 h	Initial concentration–20 mg/L Catalyst dose–0.1 g/L 25 W UV lamp	Fu et al., 2011)
1D	Nanofibers	ZnO	Ce	Hydrothermal	Vibrating absorption bands appeared at 3440 and 1630 cm^{-1} Red shift	MB	96% degradation of MB dye was observed in 420 min under the influence of visible light	Initial concentration–10 mg/L Catalyst dose–20–60 mg/50 mL Visible light (xenon lamp: 350 W, Philips, wavelength: 350–800 nm)	Shaoju et al., 2021)
-	Flower like and elliptic	ZrO_2	Ce, Er	Hydrothermal	S_{BET}: 44–66 m^2/g (specific surface area) E_g: 5.15–3.55 eV	MB	CZ05 catalyst decomposes 50% of MB dye in 3-h activity of EZ05 is about half of CZ05 in the same time	Initial concentration–7 mg/L Catalyst dose–3 g/L White LED light	Gionco et al., 2017)
3D	Hexagonal columnar	ZnO	Sr	Hydrothermal	Peak shifted towards lower angle with doping E_g: 3.22–3.18 eV	RhB	92% degradation of RhB dye in 180 min. under exposure of visible light	Initial concentration–10 mg/L Catalyst dose–50 mg/50 mL Xenon lamp (1000 W)	Li et al., 2014)
-	Nanoparticles	SnO_2	La	Sol–gel	Average crystallite size obtained to be 8.6 nm for La doped SnO_2 Red shift	Phenol	95% degradation of phenol was observed in 120 min. under exposure of UV light	Initial concentration–10 mg/L Catalyst dose–0.065 g/50 mL Reaction temp—25 °C 8 W medium-pressure mercury lamp	Al-Hamdi et al., 2014)

Table 8 (continued)

Dimension	Morphology	Parent metal oxide	Dopant	Synthesis method	Characteristics of the obtained product	Pollutant	Degradation rate	Reaction condition	Ref
0D	Nanoparticles	SnO_2	Eu	Aqueous leaf extract	Average crystallite size lies between 35 and 24 nm E_g: 3.1–3.0 eV	MO	Under UV light exposure, 90% of the MO dye degrades in 3 h	Initial concentration–20 mg/L Catalyst dose–0.15 g/100 mL UV/Visible light ($\lambda = 365$ nm) High-pressure mercury lamp (Philips, HPL-N, 250W)	Bhosale, 2019)
0D	Nanoparticles	SnO_2	Nd	Sol–gel	Specific surface area for pure and Nd-doped SnO_2 is 16 and 28 m^2/g E_g: 3.34–2.88 eV	MB	93.1% degradation of MB dye in 4 h under UV light	Initial concentration–10 µmol Catalyst dose–50 mg/100 mL Intensity of solar radiation was in the range of 700–1010 W m^{-2}	Chandran et al., 2016)
-	Nanoflowers	ZnO	Gd, La	Co-precipitation	Red shift	RhB	91% degradation of RhB dye under sunlight	Initial concentration–10 mg/L Catalyst dose–100 mg/100 mL Under direct sunlight (117,413 lx)	Palanivel et al., 2022)
-	Spherical Flakes and plates like	MgO	Gd, Er	Co-precipitation	Grain size: 43–26 nm E_g: 3.81–3.39 eV	MB, MO	97% degradation of both MB and MO	Initial concentration–35 mg/L Catalyst dose–100 mg/100 mL 125 W medium pressure mercury bulb	Vijaya Shanthi et al., 2022a)

Table 8 (continued)

Dimension	Morphology	Parent metal oxide	Dopant	Synthesis method	Characteristics of the obtained product	Pollutant	Degradation rate	Reaction condition	Ref
1D	Nanorods	WO_3	Ce	Hydrothermal	Average length and diameter: 553 and 170 nm Red shift (E_g: 2.80–2.45 eV)	RhB	96% degradation of RhB dye in 100 min. in influence of visible light	–	Govindaraj et al., 2021)
1D	Nanorods	WO_3	Eu	Hydrothermal	Average length and diameter: 90 nm and 10–17 nm Red shift	RhB, MB, MO	Under visible light, the degradation of MO, RhB, and MB dyes is 94%, 86%, and 84% in 3 h	Initial concentration–10 mg/L Catalyst dose–0.1 g/100 mL 500 W xenon lamp	Tahir et al., 2018)
-	Spherical	CeO_2	Eu	Hydrothermal	Grain size: 10–13 nm Blue shift (2.73–3.03 eV)	Congo Red	67% degradation of Congo Red dye	–	Gnanam et al., 2021)
-	Irregular	CeO_2	Gd	Simple chemical process	Particle size: 10–20 nm Blue shift (3.15–3.30 eV)	MO	Under UV light, MO dye degrades 26% in 10 min	Initial concentration–10 mg/L Catalyst dose–30 mg/30 mL UV/Visible irradiation (385 W/m^2)	Soni et al., 2021)
2D	Thin films	TiO_2	Dy, Sm, Eu	Spin coating	Thickness: 352, 356, 349, 401 nm for pure, Sm, Eu, Dy doped TiO_2 Red shift (3.32–2.65 eV)	MO	79.97%,75.4%, 58.31% degradation of MO dye by Dy, Eu, Sm doped TiO_2 in 6 h	Initial concentration–10 mg/L Catalyst dose–film was immersed /25 mL 200 W bulb	Radha et al., 2022)

Table 8 (continued)

Dimension	Morphology	Parent metal oxide	Dopant	Synthesis method	Characteristics of the obtained product	Pollutant	Degradation rate	Reaction condition	Ref
0D	Irregular	MgO	Gd	Co-precipitation	Grain size: 43–27 nm Red shift (3.81–3.43 eV)	MB, CR	92% and 88% degradation of MB and CR dyes in 160 min under UV light	Initial concentration–35 mg/L Catalyst dose–0.1 g/100 mL UV light source of Philips 125 W lamp with a wavelength of 365 nm	Vijaya Shanthi et al., 2022b)
-	Irregular	MgO	-	Green combustion	Crystallite size: 19.65 nm E_g: 3.20 eV	MG, RhB	When compared to UV light, MgO NPs exhibit greater photocatalytic activity for RhB and MG dyes	_	Anil Kumar et al., 2018)
1D	Nanorods	ZnO	Eu	Microwave assisted	Average crystallite size: 25 nm Red shift: (3.34–3.30 eV)	MO	Under UV light, MO dye degrades about 91% within 3 h	Initial concentration–0.5 to 4.0 g/L Catalyst dose–0.1 g/100 mL pH–3 to 9 High pressure mercury lamp (250 W, 365 nm)	Korake et al., 2014)
-	Spherical	ZrO_2	Eu	Co-precipitation	Particle size ranging from 8 to 30 nm Red shift (5.77–2.91 eV)	IC	Under visible light, indigo carmine dye degrades up to 64.5% in 150 min	Initial concentration–20 mg/L Catalyst dose–100 mg/100 mL 150 W ozone free xenon lamp	Agorku et al., 2015)
-	Irregular spherical	MnO_2	Eu	Sol–gel	Average grain size: 32–47 nm and diameter: 20–25 nm Red shift (3.12–2.63 eV)	MO, Phenol	97% and 87% degradation of phenol and MO dyes in 100 min under visible light	Initial concentration–5 mg/L Catalyst dose–50 mg/100 mL 500 W Xenon lamp	Panimalar et al., 2021)

Table 8 (continued)

Dimension	Morphology	Parent metal oxide	Dopant	Synthesis method	Characteristics of the obtained product	Pollutant	Degradation rate	Reaction condition	Ref
-	Irregular	SnO_2	Ce, La, Nd	Sol–gel	Average crystallite size: 8.6, 7.6, and 6.3 nm for La, Ce, Nd: SnO_2 Surface area lies between 27 and 35 m^2/g	Phenol	100%, 94.9%, 85.6% degradation of phenol by La, Nd, Ce doped SnO_2 in 120 min under UV/Vis light	Initial concentration–5 mg/L Catalyst dose–0.065 g/50 mL 8 W medium-pressure mercury lamp	Al-Hamdi et al., 2014)

Abbreviations used: MG, methyl green; MO, methyl orange; MB, methylene blue; RB, Rose Bengal; RhB, rhodamine; Nd, neodymium; Eu, europium; Y, yttrium; Sm, samarium; Er, erbium; Sr, strontium; Dy, dysprosium; E_g, band gap

radicals can be produced when excited electrons interact with adsorbed oxide species on core@shell. Furthermore, adsorbed H_2O molecules can react with holes in VB of core and shell to produce OH● radicals. Therefore, photocatalytic activity of core@shell for degradation of dye is considerably enhanced by these $O_2^{\cdot-}$, $OH^{\cdot}$, and h^+ species. These strong oxidizing agents, $OH^{\bullet}$ and $O_2^{\cdot-}$, are responsible for causing degradation of polluting dyes in non-toxic products. This demonstrates how core–shell nanoparticles (NPs) can increase production of OH● radicals by lowering the rate at which photo-induced charge carriers recombine. It supports the development of core–shell NPs' improved photocatalytic performance (Sonia et al., 2023). Table 11 depicts various semiconducting metal oxide–based core–shell nanostructures as an efficient photocatalysts.

RB dye was photodegraded under ultraviolet light to test photocatalytic performance of hematite and ceria-based core–shell nanostructures. For degradation of RB, CeO_2 and α-Fe_2O_3 were found to have very low photocatalytic activity. Because recombination and charge generation processes of pure CeO_2 and α-Fe_2O_3 are suppressed, heterojunction between two types of nanoparticles can be produced by connecting CeO_2 to α-Fe_2O_3 or vice versa. The effectiveness of photocatalyst could be enhanced by this heterojunction. When exposed to UV light for 75 min, α-Fe_2O_3@CeO_2 core–shell nanostructures showed 93% degradation of Rose Bengal dye, compared to bare CeO_2 and α-Fe_2O_3, which were 78% and 75%, respectively, as seen in Fig. 19 (Suman et al., 2021d).

Under conditions similar to sunlight, photocatalytic performance of samples of α-Fe_2O_3@SnO_2/Mxene-3.5 with various RhB dye reaction periods is investigated. The photodegradation curves of α-Fe_2O_3@SnO_2/Mxene-3.5 with various reaction times for RhB dye are shown in Fig. 20a. As reaction time increases, degradation impact also does. The photocatalytic efficiency of α-Fe_2O_3@SnO_2/Mxene-3.5 sample in 140 min (E140) can increase up to 72.43%, particularly when reaction duration was 24 h. The fitting outcomes in accordance with first-order kinetics are shown in Fig. 20b. The 24-h reaction rate constant of α-Fe_2O_3@SnO_2/Mxene-3.5 would show maximum (Zhang et al., 2022c).

Table 9 List of transition metal ion doped MONPs that are UV/Visible light active with their synthesis technique, and optical properties of particles for photocatalytic applications

Parent metal oxide	Dopant	Synthesis method	Pollutant	Degradation percentage (%)	Irradiation time	Reaction condition
ZnO	Mn	Co-precipitation	MO	85	120 min	Initial concentration–0.1 M Catalyst dose–20 mg/100 mL
ZnO	Mn	Co-precipitation	MB	87	120 min	Initial concentration–0.1 M Catalyst dose–20 mg/100 mL
ZnO	Mn	Co-precipitation	CR	86	120 min	Initial concentration–0.1 M Catalyst dose–20 mg/100 mL
ZnO	Cu	Template free reflux	MO	99.7	90 min	Initial concentration–10 mg/L Catalyst dose–50 mg/100 mL UV light (λmax = 254 nm)
ZnO	Ni	Magnetron sputtering technique	MG	100	4 h	Initial concentration–10^{-5} M Catalyst dose–50 mg/100 mL Tungsten lamp of 500 W (source of visible light ˃ 400 nm)
ZrO_2	Ni	Hydrothermal	MB	90	100 min	Initial concentration–5 mg/L Catalyst dose–15 mg/100 mL Visible-light lamp (> 400 nm) of 150 W
WO_3	Ni	Co-precipitation	MR	96	2 h	Initial concentration–10 mg/L Catalyst dose–20 mg/20 mL Visible light
ZnO	Ag	Phyto-assisted	MB	92	150 min	Initial concentration–20 mg/L Catalyst dose–20 mg/30 mL UV lamp (365 nm wavelength) 15 W
SnO_2	Ag	Co-precipitation	MB	97	120 min	Initial concentration–2.5 mol/L Catalyst dose–15 mg/25 mL UV/Vis light
SnO_2	Ni	Co-precipitation	RhB	-	-	Initial concentration–5 mg/L Catalyst dose–0.3 g/L halogen lamp source (300 W power, visible light: 400–750 nm)
SnO_2	Ni	Co-precipitation	CR	-	-	Initial concentration–5 mg/L Catalyst dose–0.3 g/L halogen lamp source (300 W power, visible light: 400–750 nm)
SnO_2	Ni	Co-precipitation	DR	-	-	Initial concentration–5 mg/L Catalyst dose–0.4 g/L halogen lamp source (300 W power, visible light: 400–750 nm)

Abbreviations used: DR, direct red; MG, methyl green

6 Conclusion

Metal oxides have been considered as potential materials for wastewater remediation due to their chemical stability, nontoxic nature, and excellent optical and electrical properties. The drawbacks of metal oxide nanoparticles/nanostructures such as wide band gap, electron–hole pair recombination, and UV irradiation working range can be significantly resolved by nanocomposites of metal

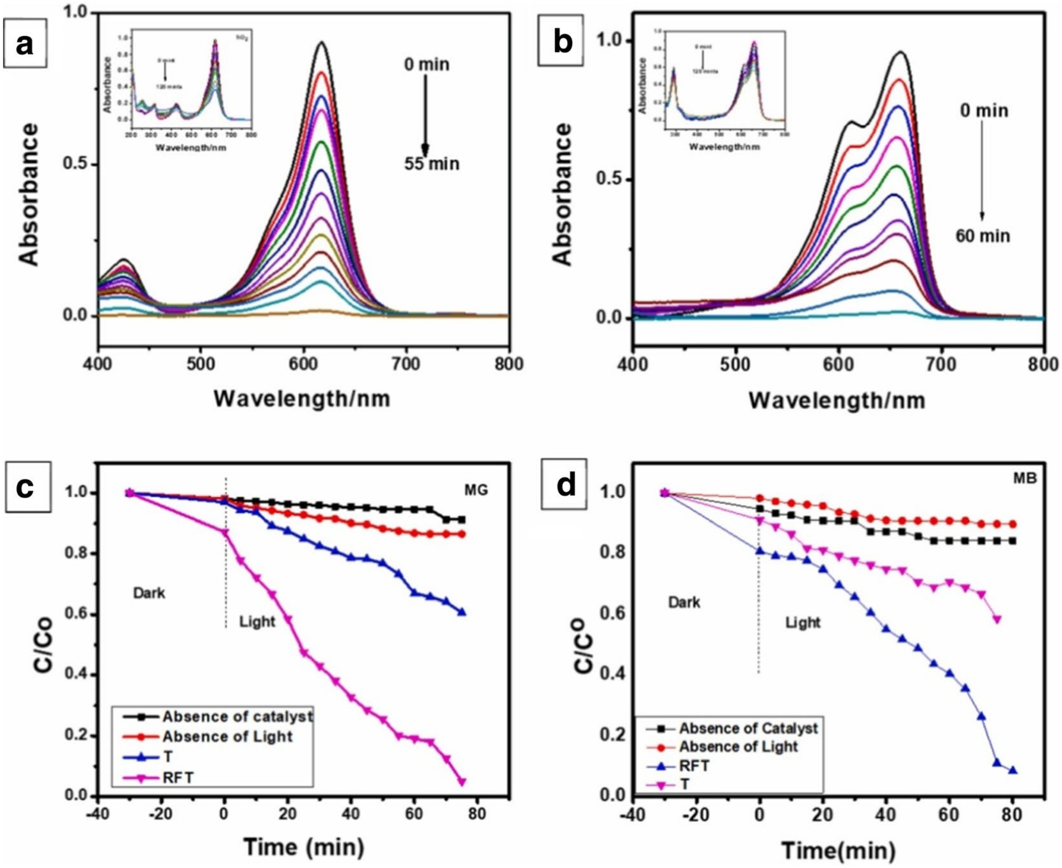

Fig. 16 Under UV/Visible irradiation absorbance spectra of MG (**a**) and MB (**b**) on a composite photocatalyst comprised of TiO_2 and rGO-Fe_3O_4 under. In absence of a catalyst and without light, comparison of photo-degradation of MG (**c**) and MB (**d**) by TiO_2(T) and rGO-Fe_3O_4/TiO_2 (RFT). Adapted from S. Bibi with license number 5554170778464

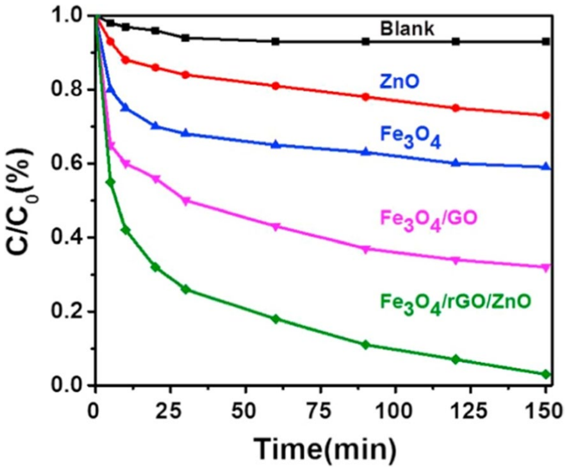

Fig. 17 Different samples degrade MB by photo-Fenton. Adapted from D. P. Ojha et al. with License number 5554160462331

oxides, their core–shell nanostructures and doping/co-doping of rare-earth as well transition metal ions. Rare-earth doping improves the optical, photocatalytic, and surface properties of nanoparticles of metal oxides. Surface defects like paramagnetic centers as well as oxygen vacancies are created due to rare-earth doping which reduces the recombination rate of electron–hole pairs. Because of these surface defects, appearance of additional visible light absorption edges takes place, which are answerable for the increment in photocatalytic performance of metal oxide photocatalysts in visible range of spectrum. Thus, this review showed the current aspects of photocatalytic process which is best economical and environment friendly way for treatment of wastewater.

Table 10 List of UV/Visible light active nanocomposites of metal oxides

Sr no	Nanocomposites	Pollutant	Degradation (%)	Time	Reaction condition	Ref
1	GO – ZnO	MB	84% in sunlight	90 min	_	Al-Rawashdeh et al., 2020)
2	GO – ZnO – Ag	MB dye	100% in sunlight	40 min	_	Al-Rawashdeh et al., 2020)
3	ZnO-PMMA	MB dye	99% in sun light	180 min	Initial concentration–2–10 mg/L Catalyst dose–25 mg/15 mL Light intensity (458 W/m^2	Rani & Shanker, 2018)
4	CeO_2/Y_2O_3	Rhodamine B dye	98% in visible light	60 min	Catalyst dose–40 mg/100 mL UV light ($\lambda < 400$ nm)	Magdalane et al., 2017)
5	CuO.ZnO.Fe_2O3/rGO	MB dye	87% under 200W low pressure bulb	80 min	Initial concentration–5 mg/L Catalyst dose–0.02 g/50 mL 200 W low pressure bulb	Fatima et al., 2020)
6	ZnO-CdO-RGO	Bisphenol A	98% in UV light	180 min	_	(Kumar et al., 2022)
7	WO_3.ZnO.NiO/CNTs	MB	66% in UV/Vis light	105 min	Initial concentration–5 mg/L catalyst dose–0.05 g/60 mL	Abo-Dief et al., 2022)
8	ZnO/CeO_2	Direct blue-15	95% under solar light	120 min	Initial concentration–50 mg/L Catalyst dose–0.05 g/100 mL Light intensity of 70 Klux	Lamba et al., 2015)
9	CeO_2/Alumina	Congo Red Methyl orange	91% in visible light 93% in visible light	120 min 90 min	Initial concentration–5 mg/L Catalyst dose–50 mg/100 mL Tungsten lamp with 300 W	Latha et al., 2017)
10	$Fe_3O_4@TiO_2$/Ag, Cu	Rhodamine B	86% under visible light	90 min	Initial concentration–10 mg/L Catalyst dose–50 mg/50 mL 500-W high-pressure mercury lamp	Ghafuri et al., 2019)
11	CeO_2/MnO_2	Methyl orange	100%	240 min	2.8 of initial pH value Catalyst dose–1.0 g/L 1.3 W/mL of ultrasonic density	Zhao et al., 2015)
13	$CuO-SnO_2$	Acid Blue 62	95% in sunlight	120 min	Initial concentration–50 mg/L^{-1} Catalyst dose–0.25 g/250 mL 500 W Xenon lamp	Li et al., 2010)

Table 10 (continued)

Sr no	Nanocomposites	Pollutant	Degradation (%)	Time	Reaction condition	Ref
14	TiO_2/SnO_2	Methylene blue	90% unser UV light	120 min	8 W mercury vapor UV light source	Karthikeyan et al., 2015)
15	$ZnO-TiO_2/rGO$	Methylene blue	99% under UV light	63 min	Initial concentration–20 mg/L Catalyst dose–20 mg/100 mL 11 W UV illuminating	Viet et al., 2021)
16	TiO_2/ZnO	2-Chlorophenol	97% under UV light	180 min	2CP with 99.5% purity Catalyst dose–12.5–50 mg/L 100 W mercury lamp	Abdel Aal et al., 2008)
17	RGO/TiO_2	Bisphenol	98% in visible light	60 min	_	Ramesh et al., 2021)
18	$NiO\text{-}SnO_2$	Bismarck brown dye	98% in sunlight	70 min	Initial concentration–15 mg/L Catalyst dose–20 mg/L 4.96 W/m^2 using a solar power meter	Begum et al., 2022)
19	ZrO_2–RGO	Nitrophenol	98% in visible light	90 min	Initial concentration–145 mg/L Catalyst dose–100 mg/L Halide lamp capacity of 400 W	Anjaneyulu, 2022)
20	$ZnO\text{-}ZrO_2$	Phenol	74% under sunlight	120 min	Initial concentration–145 mg/L Catalyst dose–200 mg/200 mL Intensity of the radiation is 90 W/m^2	Uribe López et al., 2019)

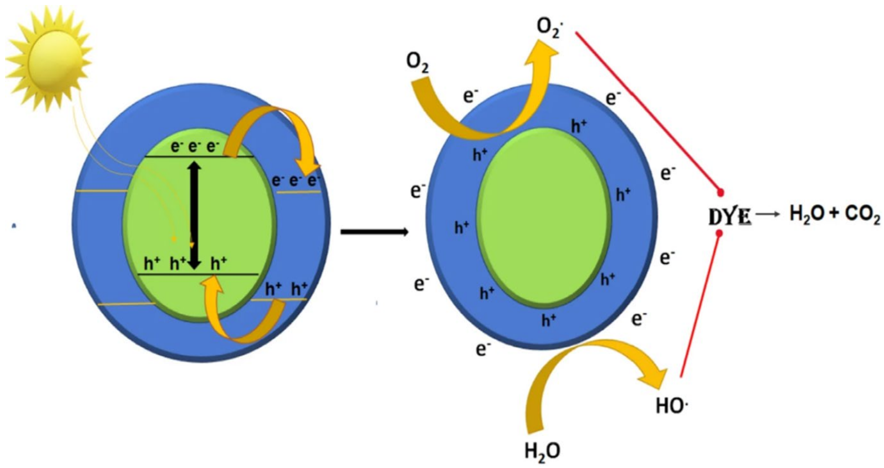

Fig. 18 Photocatalytic mechanism of core–shell nanostructure.

Table 11 List of UV/Visible light active core–shell nanostructures of metal oxides

Core–shell photocatalyst	Pollutant	Degradation (%)	Time	Light irradiated	Reaction condition	Ref
Ag–ZnO	Rhodamine B	99%	60 min	Solar light	Initial concentration–10^{-5} M Catalyst dose–20 mg/50 mL LSC-100 Solar Simulator with an AM1.5G filter	Xiong et al., 2016)
Ag-TiO_2	Methylene blue	-	-	UV	Initial concentration–10 mg/L Catalyst dose–0.02 g/200 mL UV lamp of 1.5 W	Chen & Lee, 2014)
Pt-SnO_2	Formaldehyde	93%	180 min	Visible	Catalyst dose–0.02 g Light source was an 18 W daylight lamp	Chang et al., 2014)
ZnO-TiO_2	Acridine Orange	96%	120 min	Visible and solar light	Dye solution–0.03 mM Catalyst dose–150 mg/150 mL	Balakumar & Rakkesh, 2013)
Co_3O_4@ZrO_2	Rhodamine B	_	180 min	Visible light	Catalyst dose–0.1 g/100 mL Visible light (50 W halogen light)	Shanmuganathan et al., 2020)
TiO_2/Fe_2O_3	Paracetamol	100%	90 min	UV/Vis light	Initial concentration–50 mg/L 450 W medium pressure mercury vapor lamp	Abdel-Wahab et al., 2017)
TiO_2@SnO_2	Methylene blue	71%	180 min	UV light	Dye solution–10^{-5} M Catalyst dose–0.08 g/200 mL UV lamps (Osram, 6 W, predominant peak at 254 nm)	Farhadi et al., 2017)
TiO_2@SiO_2	Methylene blue	95%	16 min	UV light	Dye solution–2×10^{-6} M Catalyst dose–10 mg 125 W high-pressure mercury lamp	Gholami et al., 2015)
ZnO:Ag	Methylene blue	~96%	90 min	UV/Vis light	Initial concentration–10 mg/L Catalyst dose–30 mg/70 mL 15W UV lamps	Jadhav & Biswas, 2018)
$NiFe_2O_4$@TiO_2	Methyl orange	90%	90 min	UV light	Initial concentration–1 mg/125 mL Catalyst dose–0.1 g/125 mL UV lamp (300 W Xenon)	Baig et al., 2020)

Table 11 (continued)

Core–shell photocatalyst	Pollutant	Degradation (%)	Time	Light irradiated	Reaction condition	Ref
$CoFe_2O_4@TiO_2$-SiO_2	Dichlorophenolindophenol (DCPIP) dye	95.32 and 87.27%	3 min	UV and visible light	MB solution–1×10^{-4} M Catalyst dose–1 g/L pH–6.7 Pressure mercury vapor source (43 W, at 254 nm	Hamad et al., 2015)
$ZnFe_2O_4@ZnO$	Methyl orange	99%	240 min	UV and visible light	Dye solution–5.6×10^{-5} M Catalyst dose–0.66 g/125 mL 4 W UV lamps	Kulkarni et al., 2016)
$CoFe_2O_4@ZnO$	Acid violet and acid brown	76% and 63%	100 min	UV light	Initial concentration–25 mg/L Catalyst dose–0.05 g/50 mL UV lamp (32 W)	Ferdosi et al., 2019)
$NiFe_2O_4@ZnO$	Congo red dye	94%	10 min	Solar light	Initial concentration–20 mg/L Catalyst dose–0.05 g/50 mL 350 W Xe arc lamp	Zhu et al., 2016)
$CoMnFe_2O_4@TiO_2$	Remazol Golden Yellow azo dye	76.3%	16 h	UV light	Initial concentration–10 mg/L Catalyst dose–10 mg/15 mL UVC lamp (E = 4.9 eV or λ = 253 nm; P = 0.5–1 W pH-6	Neris et al., 2018)
$Co_3O_4@ZrO_2$	Rhodamine B dye	_	180 min	Visible light	Catalyst dose–0.1 g/100 mL Visible light (50 W halogen light (420 nm))	Shanmuganathan et al., 2020)
ZnO/TiO_2	Methylene blue	98%	50 min	Visible light	Initial concentration–50 mg/L Catalyst dose–1 g/L A 575 W HMI lamp	Mehr et al., 2021)
Au-$WO_3@TiO_2$	Methylene blue	94.5%	240 min	Solar light	Initial concentration–30 mg/L Catalyst dose–0.02 g/100 mL 300 W Xenon lamp	Yang et al., 2020b)

7 Economic Budget of Photocatalytic Technology

- The global photocatalysts market should reach $5.1 billion by 2026 from $3.1 billion in 2021 at a compound annual growth rate (CAGR) of 10.5% for the forecast period of 2021 to 2026.
- The construction segment of global photocatalysts market is expected to grow from $2.7 billion in 2021 to $4.5 billion in 2026 at a CAGR of 10.3% for the forecast period of 2021 to 2026.
- The consumer products segment of global photocatalysts market is expected to grow from $238.7

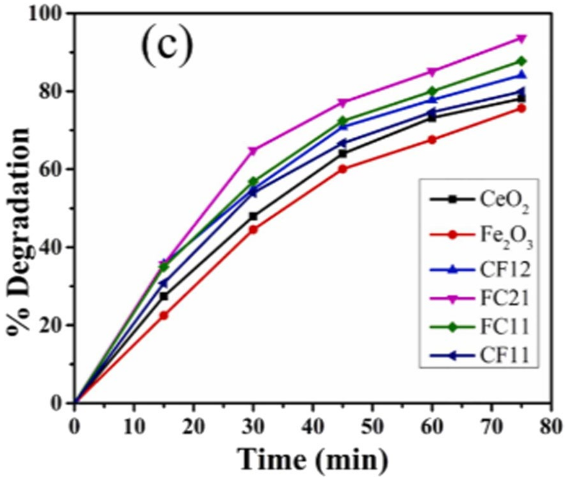

Fig. 19 % Degradation for Fe_2O_3, CeO_2, FC11, CF11, FC21, and CF12 core–shell nanoparticles at various time periods, where FC11, CF11, FC21, and CF12 represent core–shell nanostructures of α-Fe_2O_3@CeO_2 and CeO_2@α-Fe_2O_3 at different weight ratios. Adapted from Suman et al. with License number 5554160158094

> million in 2021 to $421.9 million in 2026 at a CAGR of 12.1% for the forecast period of 2021 to 2026.

In terms of material type, photocatalyst market is segmented into

- Titanium dioxide
- Tungsten trioxide-based
- Others

In terms of end use, photocatalyst market is segmented into

- Construction
- Consumer products
- Others

In terms of geography, photocatalyst market is segmented into

- North America
- Europe
- Asia-Pacific
- Rest of the World

The global market for photocatalyst-based products is expected to increase from REDACTED in 2020 to REDACTED in 2026 growing at a CAGR of REDACTED during the forecast period. Increased use in construction and consumer product sectors and in general improvement of global economic conditions is the main drivers for this expansion, which corresponds to a compound annual growth rate (CAGR) of REDACTED during the period 2020–2026. Since 2018, a marked increase in product demand has been partially offset by a significant reduction in unit prices of raw materials, resulting in lower revenues. With COVID-19 outbreak, subdued demand from construction sector has reduced demand for photocatalysts in 2021, which is expected to recover by the end of 2022. Photocatalysts are a category of catalysts that use photons to activate chemical reactions. Superior oxidizing properties and super-hydrophilicity characterize these products. Since late 1960s, these unique properties have been used in various commercial products. Although anatase titanium dioxide is most common material used to produce photocatalysts, other compounds are available (or are under development) to achieve higher photocatalytic efficiency. Photocatalysts have current and potential use across seven main industry sectors: automotive, construction, consumer products, energy, environmental, mechanical/chemical, and medical/dental.

From literature survey, electricity cost for many materials has been calculated. Table 12 shows a brief view of electricity cost in the field of photocatalysis

Fig. 20 **a** Photodegradation curves and **b** results of first-order kinetic linear fitting for various -Fe_2O_3@SnO_2/MXene-3.5 for RhB dye in sunlight-like conditions. Adapted from X. Zhang et al. with License number 5554150812650

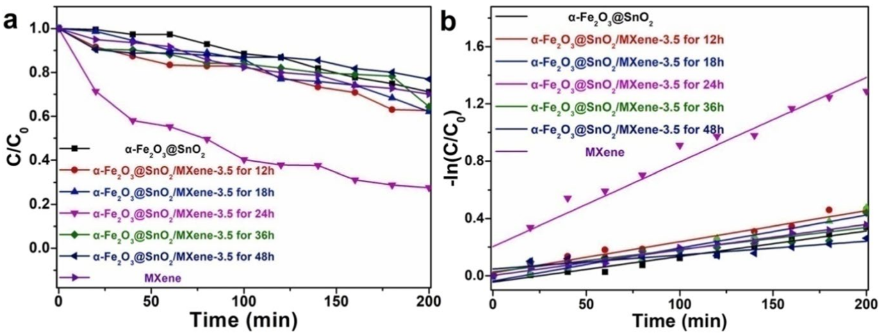

Table 12 List of electricity cost for various photocatalysts

Sr no	Photocatalyst	Morphology	Electricity cost (INR)	Ref
1	α-Fe_2O_3	Nanoparticles	2.5	Suman et al., 2021a)
2	α-Fe_2O_3	Nanoflower	2.0	Suman et al., 2021a)
3	α-Fe_2O_3	Nanocubes	2.3	Suman et al., 2021a)
4	α-Fe_2O_3/CNT7.5%	Nanoparticles	2.8	Devi et al., 2023)
5	α-Fe_2O_3/CNT 10%	Nanoparticles	2.2	Devi et al., 2023)
6	α-Fe_2O_3/Ni 4%	Flower-like	3.1	Suman et al., 2021b)
7	α-Fe_2O_3/Ni 6%	Flower like	4.4	Suman et al., 2021b)
8	CeO_2	Nanoparticles	2.58	Suman et al., 2021d)
9	α-Fe_2O_3@CeO_2 (1:2)	Core–shell	1.51	Suman et al., 2021d)
10	CeO_2@α-Fe_2O_3 (2:1)	Core–shell	2.19	Suman et al., 2021d)
11	CeO_2/Sm 0% CeO_2/Sm 4% CeO_2/Sm 6%	Nanoparticles	4.10 2.67 2.26	Chahal et al., 2020b)
12	CeO_2/La 2% CeO_2/La 4% CeO_2/La 6% CeO2/La 8%	Nanoparticles	3.37 3.14 2.60 2.44	Chahal et al., 2020a)
13	CeO_2/La 4% CeO_2/La 6% CeO_2/La 8%	Nanoparticles	2.52 2.40 1.99	Chahal et al., 2020c)

for various photocatalysts. The power consumption can be estimated using following relation:

$$t_{90} = \frac{\ln(10)}{K}$$

$$E_C = \frac{P \times t_{90} \times 4.68}{1000 \times 60}$$

where t_{90} signifies time taken by any dye to be degraded 90% of its initial concentration, E_C is electricity cost, P is power consumed (in Watt) of UV light source. Power consumers consuming a maximum 500 units of electricity per month pay INR 4.68 per unit in our locality (INR-Indian rupees).

8 Future Scope

Seeing the immense literature on photocatalytic development, it seems that nothing is left; however, still multiple problems regarding the sensible operational performances has to be enhanced. Overall to derive photocatalysis for wastewater treatment, following aspects should be under scrutiny:

1. Simplified, cost-efficient, and environment-friendly photocatalysts are required.
2. The chemical process driven by photocatalysts is not simply understood.
3. Once large-scale operations are final word factor, exploration focus ought to be directed towards the employment of extensive and noble-essence free co-catalysts.
4. The employment of these catalysts within the natural system is restricted because of low recycling capability, small size, and lower mechanical strength of these catalysts.

Acknowledgements Harita Kumari gratefully acknowledge FIST Lab, Department of Physics, Deenbandhu Chhotu Ram University of Science and Technology, Murthal, for providing research facilities.

Author Contribution All authors contributed to the study conception and design. Data collection and analysis were performed by Harita Kumari, Sonia, Suman, Seema Devi, Sourabh Sharma, and Rohit Ranga. The first draft of the manuscript was written by Harita Kumari, and all authors commented on previous versions of manuscript. Parmod Kumar, Ashok Kumar, Surjeet Chahal, Rajesh Parmar, Suresh Kumar, and Sandeep Kumar read and approved the final manuscript.

Funding Harita Kumari is financially supported by Government of India through University Grant Commission (UGC-NTA) (Ref. No. 201610156900 and Roll No. HR05603954, dated 04/02/2021). PK and SK also acknowledges the financial support by Department of Science and Technology, New Delhi for PURSE grant (SR/PURSE/2022/126).

Data Availability Not applicable.

Declarations

Conflict of Interest The authors declare no competing interests.

References

Abdel Aal, A., Barakat, M. A., & Mohamed, R. M. (2008). Electrophoreted Zn-TiO_2-ZnO nanocomposite coating films for photocatalytic degradation of 2-chlorophenol. *Applied Surface Science, 254*, 4577–4583. https://doi.org/10.1016/j.apsusc.2008.01.049

A.M. Abdel-Wahab, A.S. Al-Shirbini, O. Mohamed, & O. Nasr, (2017). Photocatalytic degradation of paracetamol over magnetic flower-like TiO_2/Fe_2O_3 core-shell nanostructures. Elsevier B.V.

Abo-Dief, H. M., Hussein, O. K., Ihsan, A., El-Bahy, S.M., Raslan, A. M., Shahid, M., & Warsi, M. F. (2022). Ternary metal oxide WO_3.NiO.ZnO nanoparticles and their composite with CNTs for organic dye photocatalytic degradation. *Ceramics International, 48*, 22269–22277. https://doi.org/10.1016/j.ceramint.2022.04.225

Abou El-Nour, K. M. M., Eftaiha, A., Al-Warthan, A., & Ammar, R. A. A. (2010). Synthesis and applications of silver nanoparticles ,Arab. *Journal Chemical, 3*, 135–140. https://doi.org/10.1016/J.ARABJC.2010.04.008

Adams, L. K., Lyon, D. Y., & Alvarez, P. J. J. (2006). Comparative eco-toxicity of nanoscale TiO_2, SiO_2, and ZnO water suspensions. *Water Research, 40*, 3527–3532. https://doi.org/10.1016/J.WATRES.2006.08.004

Adegoke, K. A., & Bello, O. S. (2015). Dye sequestration using agricultural wastes as adsorbents. *Water Resource Indian, 12*, 8–24. https://doi.org/10.1016/J.WRI.2015.09.002

Agorku, E. S., Kuvarega, A. T., Mamba, B. B., Pandey, A. C., & Mishra, A. K. (2015). Enhanced visible-light photocatalytic activity of multi-elements-doped ZrO_2 for degradation of indigo carmine. *Journal of Rare Earths, 33*, 498–506. https://doi.org/10.1016/S1002-0721(14)60447-6

Ahmad, M. A., Ahmed, N. B., Adegoke, K. A., & Bello, O. S. (2019). Sorption studies of methyl red dye removal using lemon grass (Cymbopogon citratus). *Chemical Data Collector, 22*, 100249. https://doi.org/10.1016/J.CDC.2019.100249

Ahmed, M. A., & Mohamed, A. A. (2022). Recent progress in semiconductor/graphene photocatalysts: Synthesis, photocatalytic applications, and challenges. *RSC Advances, 13*, 421–439. https://doi.org/10.1039/d2ra07225d

Akhtar, J., Tahir, M. B., Sagir, M., & Bamufleh, H. S. (2020). Improved photocatalytic performance of Gd and Nd co-doped ZnO nanorods for the degradation of methylene blue. *Ceramics International, 46*, 11955–11961. https://doi.org/10.1016/J.CERAMINT.2020.01.234

Alam, U., Khan, A., Ali, D., Bahnemann, D., & Muneer M. (2018). Comparative photocatalytic activity of sol-gel derived rare earth metal (La, Nd, Sm and Dy)-doped ZnO photocatalysts for degradation of dyes. *RSC Advances*, *8*, 17582–17594. https://doi.org/10.1039/c8ra01638k

Al-Gheethi, A. A., Azhar, Q. M., Senthil Kumar, P., Yusuf, A. A., Al-Buriahi, A. K., Radin Mohamed, R. M. S., & Al-shaibani, M. M. (2022). Sustainable approaches for removing Rhodamine B dye using agricultural waste adsorbents: A review. *Chemosphere, 287*, 132080. https://doi.org/10.1016/J.CHEMOSPHERE.2021.132080

Al-Hamdi, A. M., Sillanpää, M., & Dutta, J. (2014). Photocatalytic degradation of phenol in aqueous solution by rare earth-doped SnO_2 nanoparticles. *Journal of Materials Science, 49*, 5151–5159. https://doi.org/10.1007/s10853-014-8223-2

AliBaig, A. B., Rathinam, V., & Palaninathan, J. (2021). Facile synthesis of Ce-doped SnO_2 nanoparticles with enhanced performance for photocatalytic degradation of organic dye. *Journal Iran Chemistry Society, 18*, 13–27. https://doi.org/10.1007/s13738-020-02000-2

Al-Rawashdeh, N. A. F., Allabadi, O., & Aljarrah, M. T. (2020). Photocatalytic activity of graphene oxide/zinc oxide nanocomposites with embedded metal nanoparticles for the degradation of organic dyes. *ACS Omega, 5*, 28046–28055. https://doi.org/10.1021/acsomega.0c03608

Anil Kumar, M. R., Mahendra, B., Nagaswarupa, H. P., Surendra, B. S., Ravikumar, C. R., & Shetty, K. (2018). Photocatalytic studies of MgO nano powder; synthesized by green mediated route. *Materials Today: Proceedings*, *5*, 22221–22228. https://doi.org/10.1016/J.MATPR.2018.06.587

Anjaneyulu, R. B. (2022). Efficient photocatalytic degradation of o-nitrophenol using ZrO_2 -RGO nanocomposite: Hydrothermal approach. *Research Square*.

Baig, M. M., Pervaiz, E., & Afzal M. J. (2020). Catalytic activity and kinetic studies of core @ shell nanostructure $NiFe_2O_4@TiO_2$ for photocatalytic degradation of methyl orange dye. *Journal of the Chemical Society of Pakistan*, *42*, 04. https://doi.org/10.52568/000669

Balakumar, S., & Rakkesh, R. A. (2013). Core/shell nanostructuring of metal oxide semiconductors and their photocatalytic studies. *AIP Conference Proceedings, 1512*, 34–37. https://doi.org/10.1063/1.4790898

Bandi, V. R., Raghavan, C. M., Grandhe, B. K., Kim, S. S., Jang, K., Shin, D. S., Yi, S. S., & Jeong, J. H. (2013). Synthesis, structural and optical properties of pure and rare-earth ion doped TiO_2 nanowire arrays by a facile hydrothermal technique. *Thin Solid Films, 547*, 207–211. https://doi.org/10.1016/J.TSF.2013.03.039

Beaula Ruby Kamalam M., Inbanathan, S. S. R., Sethuraman, K., Umar, A., Algadi, H., Ibrahim, A. A., Rahman, Q. I., Garoufalis, C. S., & Baskoutas, S. (2021). Direct sunlight-driven enhanced photocatalytic performance of V_2O_5 nanorods/ graphene oxide nanocomposites for the degradation of Victoria blue dye. *Environmental Research*, *199*, 111369. https://doi.org/10.1016/j.envres.2021.111369

Begum, S., Ranjan Mishra, S., & Ahmaruzzaman, M. (2022). Facile synthesis of NiO-SnO_2 nanocomposite for enhanced photocatalytic degradation of bismarck brown. *Inorganic Chemistry Communications*, *143*, 109721. https://doi.org/10.1016/j.inoche.2022.109721

Bekris, L., Frontistis, Z., Trakakis, G., Sygellou, L., Galiotis, C., & Mantzavinos, D. (2017). Graphene: A new activator of sodium persulfate for the advanced oxidation of parabens in water. *Water Research*, *126*, 111–121. https://doi.org/10.1016/j.watres.2017.09.020

Ben Mansour, H., Ayed-Ajmi, Y., Mosrati, R., Corroler, D., Ghedira, K., Barillier, D., & Chekir-Ghedira, L. (2010). Acid violet 7 and its biodegradation products induce chromosome aberrations, lipid peroxidation, and cholinesterase inhibition in mouse bone marrow. *Environmental Science and Pollution Research*, *17*, 1371–1378. https://doi.org/10.1007/s11356-010-0323-1

Benkhaya, S., M'rabet, S., & El Harfi, A. (2020). A review on classifications, recent synthesis and applications of textile dyes. *Inorganic Chemistry Communications, 115*, 107891. https://doi.org/10.1016/J.INOCHE.2020.107891

Bhosale, T. T., Kuldeep, A. R., Pawar, S. J., Shirke, B. S., & Garadkar, K. M. (2019). Photocatalytic degradation of methyl orange by Eu doped SnO_2 nanoparticles. *Journal Material Science Material Electronic, 30,* 18927–18935. https://doi.org/10.1007/s10854-019-02249-1

Bibi, S., Ahmad, A., Anjum, M. A. R., Haleem, A., Siddiq, M., Shah, S. S., & Al Kahtani, A. (2021). Photocatalytic degradation of malachite green and methylene blue over reduced graphene oxide (rGO) based metal oxides (rGO-Fe_3O_4/TiO_2) nanocomposite under UV-visible light irradiation. *Journal Environmental Chemistry Engineering, 9*, 105580. https://doi.org/10.1016/j.jece.2021.105580

Bie, C., Zhu, B., Xu, F., Zhang, L., & Yu, J. (2019). In situ grown monolayer N-doped graphene on CdS hollow spheres with seamless contact for photocatalytic CO_2 reduction. *Advanced Materials, 31*, 1–6. https://doi.org/10.1002/adma.201902868

BilalTahir, M., & Sagir, M. (2019). Carbon nanodots and rare metals (RM = La, Gd, Er) doped tungsten oxide nanostructures for photocatalytic dyes degradation and hydrogen production. *Separate Purification Technology, 209*(2019), 94–102. https://doi.org/10.1016/J.SEPPUR.2018.07.029

Buelens, L. C., Dharanipragada, A. N. V. R., Poelman, H., Zhou, Z., Marin, G. B., & Galvita, V. V. (2019). Exploring the stability of Fe_2O_3-$MgAl_2O_4$ oxygen storage materials for CO production from CO_2. *Journal of CO_2* Utilization, *29*, 36–45. https://doi.org/10.1016/J.JCOU.2018.11.008

Chahal, S., Rani, N., Kumar, A., & Kumar, P. (2019). UV-irradiated photocatalytic performance of yttrium doped ceria for hazardous Rose Bengal dye. *Applied Surface Science, 493*, 87–93. https://doi.org/10.1016/J.APSUSC.2019.06.284

Chahal, S., Singh, S., Kumar, A., & Kumar, P. (2020a). Oxygen-deficient lanthanum doped cerium oxide nanoparticles for potential applications in spintronics and photocatalysis. *Vacuum, 177*, 109395. https://doi.org/10.1016/J.VACUUM.2020.109395

Chahal, S., Rani, N., Kumar, A., & Kumar, P. (2020b). Electronic structure and photocatalytic activity of samarium doped cerium oxide nanoparticles for hazardous rose bengal dye degradation. *Vacuum, 172*, 09075. https://doi.org/10.1016/J.VACUUM.2019.109075

Chahal, S., Kumar, A., & Kumar, P. (2020c). Erbium-doped oxygen deficient cerium oxide: Bi-functional material in the field of spintronics and photocatalysis. *Applied Nanoscience, 10*, 1721–1733. https://doi.org/10.1007/s13204-020-01253-w

Chahal, S., Phor, L., Singh, S., Singh, A., Malik, J., Goel, P., Kumar, A., Kumar, S., & Ankita, P Kumar. (2022). An efficient and unique method for the growth of spindle shaped Mg-doped cerium oxide nanorods for photodegradation of p-Nitrophenol. *Ceramics International, 48*, 28961–28968. https://doi.org/10.1016/j.ceramint.2022.04.145

Chahal, S., Phor, L., Kumar, A., Kumar, S., Kumar, S., Kumar, R., & Kumar, P. (2023). Enhanced photocatalytic degradation of organic dye by CeO_2/CNT/GO hybrid nanocomposites under UV light for wastewater treatment. *Environmental Science and Pollution Research*. https://doi.org/10.1007/s11356-023-26184-1

Chandran, D., Nair, L.S., Balachandran, S., Babu, R., & Deepa, M. (2016). Band gap narrowing and photocatalytic studies of Nd^{3+} ion-doped SnO_2 nanoparticles using solar energy. *Bulletin of Materials Science 39*, 27–33. https://doi.org/10.1007/s12034-015-1142-2

Chang, Y. C., Yan, C. Y., & Wu, R. J. (2014). Preparation of Pt@SnO_2 core-shell nanoparticles for photocatalytic degradation of formaldehyde. *Journal Chinese Chemistry Society, 61*, 345–349. https://doi.org/10.1002/jccs.201300272

Chen, Y.-W., & Lee, D.-S. (2014). Photocatalytic Destruction of Methylene Blue on Ag@TiO_2 with Core/Shell Structure. *Oalib., 01*, 1–14. https://doi.org/10.4236/oalib.1100504

Chen, N., Liu, B., Zhang, P., Wang, C., Du, Y., Chang, W., & Hong, W. (2021). Enhanced photocatalytic performance of Ce-doped SnO_2 hollow spheres by a one-pot hydrothermal method. *Inorganic Chemistry Communications, 132*, 108848. https://doi.org/10.1016/j.inoche.2021.108848

Chen, X., Li, J., & Chen, F. (2022). Photocatalytic degradation of MB by novel and environmental ZnO/Bi_2WO_6-CC hierarchical heterostructures. *Material Character, 189*, 111961. https://doi.org/10.1016/J.MATCHAR.2022.111961

Chen, D., Zhang, Y., & Chen, H. (2020). Enhancement of photo-Fenton catalytic activity with the assistance of oxalic acid on the kaolin – FeOOH system for the degradation of organic. *RSC Advances*, *10*, 18704–18714. https://doi.org/10.1039/d0ra03361h

Demartis, S., Obinu, A., Gavini, E., Giunchedi, P., & Rassu, G. (2021). Nanotechnology-based Rose Bengal: A broad-spectrum biomedical tool. *Dye Pigment, 188*, 109236. https://doi.org/10.1016/J.DYEPIG.2021.109236

Devi, S., Suman, Chahal, S., Singh, S., Ankita, Kumar, P., Kumar, S., Kumar, A., & Kumar, V. (2023). Magnetic Fe_2O_3/CNT nanocomposites: Characterization and photocatalytic application towards the degradation of Rose Bengal dye. *Ceramics International*, *49*, 20071–20079.https://doi.org/10.1016/j.ceramint.2023.03.130

Dharwal, M., Parashar, D., Shuaibu, M. S., Abdullahi, S. G., Abubakar, S., & Bala, B. B. (2020). Water pollution: Effects on health and environment of Dala LGA, Nigeria. *Material Today Process, 49*, 3036–3039. https://doi.org/10.1016/j.matpr.2020.10.496

Duan, X., Sun, H., Ao, Z., Zhou, L., Wang, G., & Wang, S. (2016). Unveiling the active sites of graphene-catalyzed peroxymonosulfate activation. *Carbon*, *107*, 371–378. https://doi.org/10.1016/j.carbon.2016.06.016

Esplugas, S., Bila, D. M., Krause, L. G. T., & Dezotti, M. (2007). Ozonation and advanced oxidation technologies to remove endocrine disrupting chemicals (EDCs) and pharmaceuticals and personal care products (PPCPs) in water effluents. *Journal of Hazardous Materials, 149*, 631–642. https://doi.org/10.1016/J.JHAZMAT.2007.07.073

Farhadi, A., Mohammadi, M. R., & Ghorbani, M. (2017). On the assessment of photocatalytic activity and charge carrier mechanism of TiO_2@SnO_2 core-shell nanoparticles for water decontamination. *Journal of Photochemistry and Photobiology, a: Chemistry, 338*, 171–177. https://doi.org/10.1016/j.jphotochem.2017.02.009

Farhan Hanafi, M., & Sapawe, N. (2020). A review on the water problem associate with organic pollutants derived from phenol, methyl orange, and remazol brilliant blue dyes. *Mater Today Process, 31*, A141–A150. https://doi.org/10.1016/J.MATPR.2021.01.258

Fatima, R., Warsi, M. F., Zulfiqar, S., Ragab, S. A., Shakir, I., & Sarwar, M. I. (2020). Nanocrystalline transition metal oxides and their composites with reduced graphene oxide and carbon nanotubes for photocatalytic applications. *Ceramics International, 46*, 16480–16492. https://doi.org/10.1016/j.ceramint.2020.03.213

Feng, Y., Su, X., Chen, Y., Liu, Y., Zhao, X., Lu, C., Ma, Y., Lu, G., & Ma, M. (2023). Research progress of graphene oxide-based magnetic composites in adsorption and photocatalytic degradation of pollutants. *A review Mater Res Bull, 162*, 112207. https://doi.org/10.1016/J.MATERRESBULL.2023.112207

Ferdosi, E., Bahiraei, H., & Ghanbari, D. (2019). Investigation the photocatalytic activity of $CoFe_2O_4$/ZnO and $CoFe_2O_4$/ZnO/Ag nanocomposites for purification of dye pollutants. *Separation and Purification Technology, 211*, 35–39. https://doi.org/10.1016/j.seppur.2018.09.054

Forgacs, E., Cserháti, T., & Oros, G. (2004). Removal of synthetic dyes from wastewaters: A review. *Environment International, 30*, 953–971. https://doi.org/10.1016/J.ENVINT.2004.02.001

Fu, M., Li, Y., Wu, S., Lu, P., Liu, J., & Dong, F. (2011). Sol–gel preparation and enhanced photocatalytic performance of Cu-doped ZnO nanoparticles. *Applied Surface Science, 258*, 1587–1591. https://doi.org/10.1016/J.APSUSC.2011.10.003

Ghafuri, H., Dehghani, M., Rashidizadeh, A., & Rabbani, M. (2019). Synthesis and characterization of magnetic nanocomposite Fe_3O_4@TiO_2/Ag, Cu and investigation of photocatalytic activity by degradation of rhodamine B (RhB) under visible light irradiation. *Optik (stuttg)., 179*, 646–653. https://doi.org/10.1016/j.ijleo.2018.10.180

Gholami, T., Bazarganipour, M., Salavati-Niasari, M., & Bagheri, S. (2015). Photocatalytic degradation of methylene blue on TiO_2@SiO_2 core/shell nanoparticles: Synthesis and characterization. *Journal of Materials Science: Materials in Electronics, 26*, 6170–6177. https://doi.org/10.1007/s10854-015-3198-6

Gionco, C., Paganini, M. C., Giamello, E., Sacco, O., Vaiano, V., & Sannino, D. (2017). Rare earth oxides in zirconium dioxide: How to turn a wide band gap metal oxide into a visible light active photocatalyst. *Journal of Energy Chemistry, 26*, 270–276. https://doi.org/10.1016/J.JECHEM.2016.07.006

Gnanam, S., Gajendiran, J., RamanaRamya, J., Ramachandran, K., & GokulRaj, S. (2021). Glycine-assisted hydrothermal synthesis of pure and europium doped CeO_2 nanoparticles and their structural, optical, photoluminescence, photocatalytic and antibacterial properties. *Chemistry Physical Letter, 763*, 138217. https://doi.org/10.1016/J.CPLETT.2020.138217

Gopal, G., Alex, S. A., Chandrasekaran, N., & Mukherjee, A. (2020). A review on tetracycline removal from aqueous systems by advanced treatment techniques. *RSC Advances, 10*, 27081–27095. https://doi.org/10.1039/d0ra04264a

Govindaraj, T., Mahendran, C., Manikandan, V. S., Archana, J., & Navaneethan, M. (2021). Enhanced visible-light-driven photocatalytic activity of Ce doped WO3 nanorods for Rhodamine B dye degradation. *Material Letter, 305*, 130705. https://doi.org/10.1016/J.MATLET.2021.130705

Hamad, H., Abd El-Latif, M., Kashyout, A. E. H., Sadik, W., & Feteha, M. (2015). Synthesis and characterization of core-shell-shell magnetic ($CoFe_2O_4$-SiO_2-TiO_2) nanocomposites and TiO_2 nanoparticles for the evaluation of photocatalytic activity under UV and visible irradiation, New. *Journal Chemistry, 39*, 3116–3128. https://doi.org/10.1039/c4nj01821d

Hao, M., Qiu, M., Yang, H., Hu, B., & Wang, X. (2021). Recent advances on preparation and environmental applications of MOF-derived carbons in catalysis. *Science Total Environmental, 760*, 143333. https://doi.org/10.1016/j.scitotenv.2020.143333

He, X., Yang, D. P., Zhang, X., Liu, M., Kang, Z., Lin, C., Jia, N., & Luque, R. (2019). Waste eggshell membrane-templated CuO-ZnO nanocomposites with enhanced adsorption, catalysis and antibacterial properties for water purification. *Chemical Engineering Journal, 369*, 621–633. https://doi.org/10.1016/j.cej.2019.03.047

He, J., Wan, Y., & Zhou, W. (2021). ZIF-8 derived Fe-N coordination moieties anchored carbon nanocubes for efficient peroxymonosulfate activation via non-radical pathways: Role of FeNx sites. *Journal Hazardous Material, 405*, 124199. https://doi.org/10.1016/j.jhazmat.2020.124199

He, Q., Xie, C., Gan, D., & Xiao, C. (2020). The efficient degradation of organic pollutants in an aqueous environment under visible light irradiation by persulfate catalytically activated with kaolin-Fe2O3. *RSC Advances*, *10*, 43–52. https://doi.org/10.1039/c9ra09253f

Hernández-Zamora, M., & Martínez-Jerónimo, F. (2019). Exposure to the azo dye Direct blue 15 produces toxic effects on microalgae, cladocerans, and zebrafish embryos. *Ecotoxicology, 28*, 890–902. https://doi.org/10.1007/s10646-019-02087-1

Hethnawi, A., Nassar, N. N., Manasrah, A. D., & Vitale, G. (2017). Polyethylenimine-functionalized pyroxene nanoparticles embedded on diatomite for adsorptive removal of dye from textile wastewater in a fixed-bed column. *Chemical Engineering Journal, 320*, 389–404. https://doi.org/10.1016/J.CEJ.2017.03.057

Holkar, C. R., Jadhav, A. J., Pinjari, D. V., Mahamuni, N. M., & Pandit, A. B. (2016). A critical review on textile wastewater treatments: Possible approaches. *Journal of Environmental Management, 182*, 351–366. https://doi.org/10.1016/J.JENVMAN.2016.07.090

Hosseini, Z. S., Haghparast, F., Masoudi, A. A., & Mortezaali, A. (2022). Enhanced visible photocatalytic performance of un-doped TiO_2 nanoparticles thin films through modifying the substrate surface roughness. *Material Chemistry Physical, 279*, 125530. https://doi.org/10.1016/J.MATCHEMPHYS.2021.125530

Hu, X., Zhang, Y., Wang, B., Li, H., & Dong, W. (2019). Novel g-C_3N_4/$BiOCl_xI_{1-x}$ nanosheets with rich oxygen vacancies for enhanced photocatalytic degradation of organic contaminants under visible and simulated solar light. *Applied Catalysis B Environmental, 256*, 117789. https://doi.org/10.1016/j.apcatb.2019.117789

Hu, M., Yao, Z., & Wang, X. (2017). Graphene-based nanomaterials for catalysis. Industrial & Engineering Chemistry Research, *56*, 3477–3502. https://doi.org/10.1021/acs.iecr.6b05048

Hu, Y., Chen, D., Zhang, R., Ding, Y., Ren, Z., Fu, M., Cao, X., & Zeng, G. (2021). Singlet oxygen-dominated activation of peroxymonosulfate by passion fruit shell derived biochar for catalytic degradation of tetracycline through a non-radical oxidation pathway. *Journal Hazardous Material*, *419*, 126495. https://doi.org/10.1016/j.jhazmat.2021.126495

Huang, D., Yan, X., Yan, M., Zeng, G., Zhou, C., Wan, J., Cheng, M., & Xue, W. (2018). Graphitic carbon nitride-based heterojunction photoactive nanocomposites: Applications and mechanism insight. *ACS Applied Materials & Interfaces, 10*, 21035–21055. https://doi.org/10.1021/acsami.8b03620

Huang, R., Lin, Q., Zhong, Q., Zhang, X., Wen, X., & Luo, H. (2020). Removal of Cd(II) and Pb(II) from aqueous solution by modified attapulgite clay. *Arabian Journal of Chemistry, 13*, 4994–5008. https://doi.org/10.1016/J.ARABJC.2020.01.022

Huang, Y., Li, J., Du, P., & Lu, X. (2021a). Rational design of copper encapsulated within nitrogen-doped carbon core-shell nanosphere for efficiently photocatalytic peroxymonosulfate activation. *Journal of Colloid and Interface Science, 597*, 206–214. https://doi.org/10.1016/j.jcis.2021.04.016

Huang, W., Xiao, S., Zhong, H., Yan, M., & Yang, X. (2021b). Activation of persulfates by carbonaceous materials: A review. *Chemistry Engineering Journal, 418*, 129297. https://doi.org/10.1016/j.cej.2021.129297

Huang, D., Zhang, G., Yi, J., Cheng, M., Lai, C., Xu, P., Zhang, C., Liu, Y., Zhou, C., Xue, W., Wang, R., Li, Z., & Chen, S. (2021c). Progress and challenges of metal-organic frameworks-based materials for SR-AOPs applications in water treatment. *Chemosphere, 263*, 127672. https://doi.org/10.1016/j.chemosphere.2020.127672

Huo, X., Zhou, P., Liu, Y., Cheng, F., Liu, Y., Cheng, X., Zhang, Y., & Wang, Q. (2020). Removal of contaminants by activating peroxymonosulfate (PMS) using zero valent iron (ZVI)-based bimetallic particles (ZVI/Cu, ZVI/Co, ZVI/Ni, and ZVI/Ag). *RSC Advances, 10*, 28232–28242. https://doi.org/10.1039/d0ra03924a

Jadhav, J., & Biswas, S. (2018). Hybrid ZnO: Ag core-shell nanoparticles for wastewater treatment: Growth mechanism and plasmonically enhanced photocatalytic activity. *Applied Surface Science, 456*, 49–58. https://doi.org/10.1016/j.apsusc.2018.06.028

Janbandhu, S. Y., Munishwar, S. R., Sukhadeve, G. K., & Gedam, R. S. (2019). Effect of annealing time on optical properties of CdS QDs containing glasses and their application for degradation of methyl orange dye. *Materials Characterization, 152*, 230–238. https://doi.org/10.1016/J.MATCHAR.2019.04.027

Joshi, N. C., Gururani, P., & Gairola, S. P. (2022). Metal oxide nanoparticles and their nanocomposite-based materials as photocatalysts in the degradation of dyes. *Biointerface Research Applied Chemical, 12*, 6557–6579. https://doi.org/10.33263/BRIAC125.65576579

Kapoor, R. T., Danish, M., Singh, R. S., Rafatullah, M., & Abdul, A. K. (2021). Exploiting microbial biomass in treating azo dyes contaminated wastewater: Mechanism of degradation and factors affecting microbial efficiency. *Journal of Water Process Engineering, 43*, 102255. https://doi.org/10.1016/J.JWPE.2021.102255

Karimi-Maleh, H., Kumar, B. G., Rajendran, S., Qin, J., Vadivel, S., Durgalakshmi, D., Gracia, F., Soto-Moscoso, M., Orooji, Y., & Karimi, F. (2020). Tuning of metal oxides photocatalytic performance using Ag nanoparticles integration. *Journal Molecular Liqud, 314*, 113588. https://doi.org/10.1016/J.MOLLIQ.2020.113588

Karthikeyan, N., Narayanan, V., & Stephen, A. (2015). Degradation of textile effluent using nanocomposite TiO_2/SnO_2 semiconductor photocatalysts. *International Journal of ChemTech Research, 8*, 443–449.

Katheresan, V., Kansedo, J., & Lau, S. Y. (2018). Efficiency of various recent wastewater dye removal methods: A review. *Journal of Environmental Chemical Engineering, 6*, 4676–4697. https://doi.org/10.1016/J.JECE.2018.06.060

Keerthana, S. P., Yuvakkumar, R., Kumar, P. S., Ravi, G., & Velauthapillai, D. (2021). Rare earth metal (Sm) doped zinc ferrite ($ZnFe_2O_4$) for improved photocatalytic elimination of toxic dye from aquatic system.

Environmental Research, 197, 111047. https://doi.org/10.1016/J.ENVRES.2021.111047

Klein, S., Worch, E., & Knepper, T. P. (2015). Occurrence and spatial distribution of microplastics in river shore sediments of the rhine-main area in Germany. *Environmental Science and Technology, 49*, 6070–6076. https://doi.org/10.1021/acs.est.5b00492

Korake, P. V., Kadam, A. N., & Garadkar, K. M. (2014). Photocatalytic activity of Eu^{3+}-doped ZnO nanorods synthesized via microwave assisted technique. *Journal of Rare Earths, 32*, 306–313. https://doi.org/10.1016/S1002-0721(14)60072-7

Kulkarni, S. D., Kumbar, S., Menon, S. G., Choudhari, K. S., & Santhosh, C. (2016). Magnetically separable core-shell $ZnFe_2O_4$@ZnO nanoparticles for visible light photodegradation of methyl orange. *Materials Research Bulletin, 77*, 70–77. https://doi.org/10.1016/j.materresbull.2016.01.022

Kumar, L., Ragunathan, V., Mohita Chugh, N., & Bharadvaja. (2021). Nanomaterials for remediation of contaminants: a review. *Environmental Chemical Letter, 19*, 3139–3163. https://doi.org/10.1007/s10311-021-01212-z

Kumar, S., Kaushik, R. D., & Purohit, L. P. (2022). ZnO-CdO nanocomposites incorporated with graphene oxide nanosheets for efficient photocatalytic degradation of bisphenol A, thymol blue and ciprofloxacin. *Journal Hazardous Material*, *424*, 127332. https://doi.org/10.1016/j.jhazmat.2021.127332

Lamba, R., Umar, A., Mehta, S. K., & Kansal, S. K. (2015). CeO_2ZnO hexagonal nanodisks: Efficient material for the degradation of direct blue 15 dye and its simulated dye bath effluent under solar light. *Journal of Alloys and Compounds, 620*, 67–73. https://doi.org/10.1016/j.jallcom.2014.09.101

Latha, P., Prakash, K., & Karuthapandian, S. (2017). Enhanced visible light photocatalytic activity of CeO_2/alumina nanocomposite: Synthesized via facile mixing-calcination method for dye degradation. *Advanced Powder Technology, 28*, 2903–2913. https://doi.org/10.1016/j.apt.2017.08.017

Lellis, B., Fávaro-Polonio, C. Z., Pamphile, J. A., & Polonio, J. C. (2019). Effects of textile dyes on health and the environment and bioremediation potential of living organisms. *Biotechnology Research Innovations, 3*, 275–290. https://doi.org/10.1016/J.BIORI.2019.09.001

Li, D., Huang, J. F., Cao, L. Y., Li, J. Y., Ouyang, H. B., & Yao, C. Y. (2014). Microwave hydrothermal synthesis of Sr2+ doped ZnO crystallites with enhanced photocatalytic properties. *Ceramics International, 40*, 2647–2653. https://doi.org/10.1016/J.CERAMINT.2013.10.061

Li, X., Guo, W., Liu, Z., Wang, R., & Liu, H. (2016). Applied Surface Science Fe-based MOFs for efficient adsorption and degradation of acid orange 7 in aqueous solution via persulfate activation. *Applied Surface Science, 369*, 130–136. https://doi.org/10.1016/j.apsusc.2016.02.037

Li, H., Sun, S., Ji, H., Liu, W., & Shen, Z. (2020). Enhanced activation of molecular oxygen and degradation of tetracycline over $Cu-S_4$ atomic clusters. *Applied Catalysis B Environmental, 272*, 118966. https://doi.org/10.1016/j.apcatb.2020.118966

Li, J., Huang, L., Jiang, X., Zhang, L., & Sun, X. (2021). Preparation and characterization of ternary $Cu/Cu_2O/C$ composite: An extraordinary adsorbent for removing anionic organic dyes from water. *Chemical Engineering Journal, 404*, 127091. https://doi.org/10.1016/j.cej.2020.127091

Li, L., Zhuang, H.S., Bu, D. (2010). Photocatalytic degradation of acid blue 62 over $La/I/TiO_2$ nanocomposite photocatalyst under simulated sunlight, J. Donghua Univ. (English Ed. 27 760–763.

Li, J., Xiao, C., Wang, K., Li, Y., & Zhang, G. J. (2019). Accepted, enhanced generation of reactive oxygen species under visible light irradiation by adjusting the exposed facet of $FeWO_4$ nanosheets to activate oxalic acid for organic pollutant removal and Cr (VI) reduction. *Environmental Science Technology*, *53*, 11023–11030. https://doi.org/10.1021/acs.est.9b00641

Liu, C., Wang, Y., Zhang, Y., Li, R., Meng, W., Song, Z., Qi, F., Xu, B., Chu, W., Yuan, D., & Yu, B. (2018). Enhancement of Fe@porous carbon to be an efficient mediator for peroxymonosulfate activation for oxidation of organic contaminants: Incorporation NH_2-group into structure of its MOF precursor. *Chemical Engineering Journal, 354*, 835–848. https://doi.org/10.1016/j.cej.2018.08.060

Liu, J., Wang, P., Qu, W., Li, H., Shi, L., & Zhang, D. (2019). Nanodiamond-decorated ZnO catalysts with enhanced photocorrosion-resistance for photocatalytic degradation of gaseous toluene. *Applied Catalysis B: Environmental*, *257*, 117880. https://doi.org/10.1016/j.apcatb.2019.117880

Lundström, S. V., Östman, M., Bengtsson-Palme, J., Rutgersson, C., Thoudal, M., Sircar, T., Blanck, H., Eriksson, K. M., Tysklind, M., Flach, C. F., & Larsson, D. G. J. (2016). Minimal selective concentrations of tetracycline in complex aquatic bacterial biofilms. *Science of the Total Environment, 553*, 587–595. https://doi.org/10.1016/j.scitotenv.2016.02.103

Luo, H., Fu, H., Yin, H., & Lin, Q. (2022). Carbon materials in persulfate-based advanced oxidation processes: The roles and construction of active sites. *Journal Hazardous Material, 426*, 128044. https://doi.org/10.1016/J.JHAZMAT.2021.128044

Magdalane, C. M., Kaviyarasu, K., Vijaya, J. J., Siddhardha, B., Jeyaraj, B., Kennedy, J., & Maaza, M. (2017). Evaluation on the heterostructured CeO_2/Y_2O_3 binary metal oxide nanocomposites for UV/Vis light induced photocatalytic degradation of Rhodamine - B dye for textile engineering application. *Journal of Alloys and Compounds, 727*, 1324–1337. https://doi.org/10.1016/j.jallcom.2017.08.209

Manavi, N., Kazemi, A. S., & Bonakdarpour, B. (2017). The development of aerobic granules from conventional activated sludge under anaerobic-aerobic cycles and their adaptation for treatment of dyeing wastewater. *Chemical Engineering Journal, 312*, 375–384. https://doi.org/10.1016/J.CEJ.2016.11.155

Mehr, M. E., Maleki-Ghaleh, H., Yarahmadi, M., Kavanlouei, M., & Siadati, M. H. (2021). Synthesis and characterization of photocatalytic zinc oxide/titanium oxide (core/shell) nanocomposites. *Journal Alloys*

Compound, 882, 160777. https://doi.org/10.1016/j.jallcom.2021.160777

Mohammadi, N., Khani, H., Gupta, V. K., Amereh, E., & Agarwal, S. (2011). Adsorption process of methyl orange dye onto mesoporous carbon material–kinetic and thermodynamic studies. *Journal of Colloid and Interface Science, 362*, 457–462. https://doi.org/10.1016/J.JCIS.2011.06.067

Naseem, T., & Durrani, T. (2021). The role of some important metal oxide nanoparticles for wastewater and antibacterial applications: A review. *Environmental Chemistry Ecotoxicology, 3*, 59–75. https://doi.org/10.1016/J.ENCECO.2020.12.001

Naseem, K., Farooqi, Z. H., Begum, R., & Irfan, A. (2018). Removal of Congo red dye from aqueous medium by its catalytic reduction using sodium borohydride in the presence of various inorganic nano-catalysts: A review. *Journal of Cleaner Production, 187*, 296–307. https://doi.org/10.1016/J.JCLEPRO.2018.03.209

Neris, A. M., Schreiner, W. H., Salvador, C., Silva, U. C., Chesman, C., Longo, E., & Santos, I. M. G. (2018). Photocatalytic evaluation of the magnetic core@shell system (Co, Mn)Fe_2O_4@TiO_2 obtained by the modified Pechini method. Mater. *Science Engineering B Solid-State Material Advance Technology, 229*, 218–226. https://doi.org/10.1016/j.mseb.2017.12.029

Oh, W., & Lim, T. (2018). Design and application of heterogeneous catalysts as peroxydisulfate activator for organics removal : An overview. *Chemical Engineering Journal, 358, 110–133.* https://doi.org/10.1016/j.cej.2018.09.203

Ojha, D. P., Joshi, M. K., & Kim, H. J. (2017). Photo-Fenton degradation of organic pollutants using a zinc oxide decorated iron oxide/reduced graphene oxide nanocomposite. *Ceramics International, 43*, 1290–1297. https://doi.org/10.1016/j.ceramint.2016.10.079

Palanivel, B., Macadangdang, R. R., Hossain, M. S., Alharthi, F. A., Kumar, M., Chang, J.-H., & Gedi, S. (2022). Rare earth (Gd, La) co-doped ZnO nanoflower for direct sunlight driven photocatalytic activity. *Journal of Rare Earths, 41, 77–84.* https://doi.org/10.1016/J.JRE.2022.01.009

Panimalar, S., Chandrasekar, M., Logambal, S., Uthrakumar, R., & Inmozhi, C. (2021). Europium-doped MnO_2 nanostructures for controlling optical properties and visible light photocatalytic activity. *Material Today Processing, 56, 3394-3401.* https://doi.org/10.1016/J.MATPR.2021.10.335

Park, J. S., Kim, B. J., Seo, B. G., Han, G. D., Park, K. H., Koo, J., Park, H. D., & Shim, J. H. (2022). Heterostructured palladium-coated zinc oxide photocatalysts for sustainable water treatment. *Journal Water Process Engineering, 45*, 102488. https://doi.org/10.1016/J.JWPE.2021.102488

Pascariu, P., Cojocaru, C., Olaru, N., Samoila, P., Airinei, A., Ignat, M., Sacarescu, L., & Timpu, D. (2019). Novel rare earth (RE-La, Er, Sm) metal doped ZnO photocatalysts for degradation of Congo-Red dye: Synthesis, characterization and kinetic studies. *Journal of Environmental Management, 239*, 225–234. https://doi.org/10.1016/J.JENVMAN.2019.03.060

Perumal, V., Inmozhi, C., Uthrakumar, R., Robert, R., Chandrasekar, M., Mohamed, S. B., Honey, S., Raja, A., Al-Mekhlafi, F. A., & Kaviyarasu, K. (2022). Enhancing the photocatalytic performance of surface - Treated SnO_2 hierarchical nanorods against methylene blue dye under solar irradiation and biological degradation. *Environmental Research, 209*, 112821. https://doi.org/10.1016/J.ENVRES.2022.112821

Radha, E., Komaraiah, D., Sayanna, R., & Sivakumar, J. (2022). Photoluminescence and photocatalytic activity of rare earth ions doped anatase TiO_2 thin films. *Journal Luminescence, 244*, 118727. https://doi.org/10.1016/J.JLUMIN.2022.118727

Raizada, P., Soni, V., Kumar, A., Singh, P., Parwaz Khan, A. A., Asiri, A. M., Thakur, V. K., & Nguyen, V. H. (2021). Surface defect engineering of metal oxides photocatalyst for energy application and water treatment. *Journal Material, 7*, 388–418. https://doi.org/10.1016/J.JMAT.2020.10.009

Rajendiran, R., Patchaiyappan, A., Harisingh, S., Balla, P., Paari, A., Ponnala, B., Perupogu, V., Lassi, U., & Seelam, P. K. (2022). Synergistic effects of graphene oxide grafted chitosan & decorated MnO_2 nanorods composite materials application in efficient removal of toxic industrial dyes. *Journal Water Process Engineering, 47*, 102704. https://doi.org/10.1016/J.JWPE.2022.102704

Ramesh, K., Gnanavel, B., & Shkir, M. (2021). Enhanced visible light photocatalytic degradation of bisphenol A (BPA) by reduced graphene oxide (RGO)–metal oxide (TiO_2, ZnO and WO_3) based nanocomposites. *Diamond Relate Material, 118*, 108514. https://doi.org/10.1016/j.diamond.2021.108514

Rachna, Rani, M., Shanker, U., SC, (2019). Degradation of tricyclic polyaromatic hydrocarbons in water, soil and river sediment with a novel TiO2 based heterogeneous nanocomposite. *Journal of Environmental Management*, *248*, 109340.

Rani, N., Chahal, S., Mahadevan, S. K., Kumar, P., Shukla, R., & Singh, S. K. (2020). Development of hierarchical magnesium oxide anchored cerium oxide nanocomposites with improved magnetic properties and photocatalytic performance. *Nanotechnology*, *31*, 374004. https://doi.org/10.1088/1361-6528/ab96e8

Rani, M., & Shanker, U. (2018). Sun-light driven rapid photocatalytic degradation of methylene blue by poly(methyl methacrylate)/metal oxide nanocomposites. *Colloids Surfaces A Physicochemistry Engineering Asp, 559*, 136–147. https://doi.org/10.1016/j.colsurfa.2018.09.040

Rani, M., & Shanker, U. (2021). Synergistic effects of zinc oxide coupled copper hexacyanoferrate nanocomposite : Robust visible-light driven dye degradation. *Journal of Colloid and Interface Science, 584*, 67–79. https://doi.org/10.1016/j.jcis.2020.09.079

Rehman, S., Ullah, R., Butt, A. M., & Gohar, N. D. (2009). Strategies of making TiO_2 and ZnO visible light active. *Journal of Hazardous Materials, 170*, 560–569. https://doi.org/10.1016/J.JHAZMAT.2009.05.064

Salleh, M. A. M., Mahmoud, D. K., Karim, W. A. W. A., & Idris, A. (2011). Cationic and anionic dye adsorption by agricultural solid wastes: A comprehensive review.

Desalination, 280, 1–13. https://doi.org/10.1016/J.DESAL.2011.07.019

Semeraro, P., Rizzi, V., Fini, P., Matera, S., Cosma, P., Franco, E., García, R., Ferrándiz, M., Núñez, E., Gabaldón, J. A., Fortea, I., Pérez, E., & Ferrándiz, M. (2015). Interaction between industrial textile dyes and cyclodextrins. *Dyes and Pigments, 119*, 84–94. https://doi.org/10.1016/J.DYEPIG.2015.03.012

Shaheen, K., Suo, H., Arshad, T., Shah, Z., Khan, S. A., Khan, S. B., Khan, M. N., Liu, M., Ma, L., Cui, J., Ji, Y. T., & Wang, Y. (2020). Metal oxides nanomaterials for the photocatalytic mineralization of toxic water wastes under solar light illumination. *Journal of Water Processing Engineering, 34*, 101138. https://doi.org/10.1016/J.JWPE.2020.101138

Shanmuganathan, R., LewisOscar, F., Shanmugam, S., Thajuddin, N., Alharbi, S. A., Alharbi, N. S., Brindhadevi, K., & Pugazhendhi, A. (2020). Core/shell nanoparticles: Synthesis, investigation of antimicrobial potential and photocatalytic degradation of Rhodamine B. *Journal Photochemical Photobiology B Biology, 202*, 111729. https://doi.org/10.1016/j.jphotobiol.2019.111729

Shaoju, J., Zhiwei, T., Kaiyin, Z., Gaigai, D., Weisen, Y., & Shaohua, J. (2021). Hydrothermal synthesis of Ce-doped ZnO heterojunction supported on carbon nanofibers with high visible light photocatalytic activity. *Chemistry Research Chinese University, 37*, 565–570. https://doi.org/10.1007/s40242-021-1114-6

Shon, H. K., Vigneswaran, S., & Snyder, S. A. (2007). Effluent organic matter (EfOM) in wastewater: Constituents, effects, and treatment effluent organic matter (EfOM) in wastewater. *Critical Reviews in Environmental Science and Technology*, *36*, 327–374. https://doi.org/10.1080/10643380600580011

Singh, K., Harish, S., Kristy, A. P., Shivani, V., Archana, J., Navaneethan, M., Shimomura, M., & Hayakawa, Y. (2018). Erbium doped TiO_2 interconnected mesoporous spheres as an efficient visible light catalyst for photocatalytic applications. *Applied Surface Science, 449*, 755–763. https://doi.org/10.1016/J.APSUSC.2018.01.279

Sivakumar, V., Anna, J. L., Vijayeeswarri, J., & Swaminathan, G. (2009). Ultrasound assisted enhancement in natural dye extraction from beetroot for industrial applications and natural dyeing of leather. *Ultrasonics Sonochemistry, 16*, 782–789. https://doi.org/10.1016/J.ULTSONCH.2009.03.009

Soares, G. M. B., De Amorim, M. T. P., & Costa-Ferreira, M. (2001). Use of laccase together with redox mediators to decolourize Remazol Brilliant Blue R. *Journal of Biotechnology, 89*, 123–129. https://doi.org/10.1016/S0168-1656(01)00302-9

Sodhi, M., & Etminan, M. (2020). Therapeutic potential for tetracyclines in the treatment of COVID-19. *Pharmacotherapy, 40*, 487–488. https://doi.org/10.1002/phar.2395

Solayman, H. M., Hossen, M. A., Abd Aziz, A., Yahya, N. Y., Leong, K. H., Sim, L. C., Monir, M. U., & Zoh, K. D. (2023). Performance evaluation of dye wastewater treatment technologies: A review. *Journal Environmental Chemical. Engineering, 11*, 109610. https://doi.org/10.1016/J.JECE.2023.109610

Soni, B., Makkar, S., & Biswas, S. (2021). Effects of surface structure and defect behavior on the magnetic, electrical, and photocatalytic properties of Gd-doped CeO_2 nanoparticles synthesized by a simple chemical process. *Material Character, 174*, 110990. https://doi.org/10.1016/J.MATCHAR.2021.110990

Sonia, H. Kumari, Suman, Chahal, S., Devi, S., Kumar, S., Kumar, S., P., & Kumar, A. (2023). Spinel ferrites/metal oxide nanocomposites for waste water treatment. *Applied Physics A Materials Science & Processing*, *129*. https://doi.org/10.1007/s00339-022-06288-0

Srinivasan, A., & Viraraghavan, T. (2010). Decolorization of dye wastewaters by biosorbents: A review. *Journal of Environmental Management, 91*, 1915–1929. https://doi.org/10.1016/J.JENVMAN.2010.05.003

Štengl, V., Bakardjieva, S., & Murafa, N. (2009). Preparation and photocatalytic activity of rare earth doped TiO_2 nanoparticles. *Materials Chemistry and Physics, 114*, 217–226. https://doi.org/10.1016/J.MATCHEMPHYS.2008.09.025

Suman, S., Chahal, A., & Kumar, P. (2020b). Kumar, Annealing effect on photocatalytic and magnetic properties of Zn doped hematite nanoparticles. *AIP Conference Proceedings, 2265*, 3–7. https://doi.org/10.1063/5.0016664

Suman, Devi, S., Sharma, V., Chahal, S., Goel, P., Singh, S., Kumar, A., & Kumar, P. (2021). Phase transformation and structural evolution in iron oxide nanostructures. *Material Science Engineering B, 272*, 115329. https://doi.org/10.1016/j.mseb.2021.115329

Suman, Chahal, S., Singh, S., Goel, P., Kumar, A., Singh, O., & Kumar, P. (2021b). Understanding the role of Ni ions on the photocatalytic activity and dielectric properties of hematite nanostructures: An experimental and DFT approach. *Journal Physical Chemistry Solids, 156*, 110118. https://doi.org/10.1016/j.jpcs.2021.110118

Suman, T., Sharma, V., Devi, S., Chahal, S., Singh, J. P., Chae, K. H., Kumar, A., Asokan, K., & Kumar, P. (2021c). Phase transformation in Fe_2O_3 nanoparticles: Electrical properties with local electronic structure. *Physical B Condensation Matter, 620*, 413275. https://doi.org/10.1016/j.physb.2021.413275

Suman, S., Chahal, A., Kumar, P., Kumar. (2020a). Zn doped α-Fe_2O_3: An efficient material for UV driven photocatalysis and electrical conductivity. *Crystals*, *10*, 273. https://doi.org/10.3390/cryst10040273

Suman, S. Singh, Ankita, Kumar, A., Kataria, N., Kumar, S., & Kumar, P. (2021d). Photocatalytic activity of α-Fe_2O_3@CeO_2 and CeO_2@α-Fe_2O_3 core-shell nanoparticles for degradation of Rose Bengal dye. *Journal of Environmental Chemical Engineering*, *9*, 106266. https://doi.org/10.1016/j.jece.2021.106266

Tahir, M. B., Nabi, G., Khalid, N. R., & Rafique, M. (2018). Role of europium on WO_3 performance under visible-light for photocatalytic activity. *Ceramics International, 44*, 5705–5709. https://doi.org/10.1016/J.CERAMINT.2017.12.223

Tang, J., & Wang, J. (2019). MOF-derived three-dimensional flower-like FeCu@C composite as an efficient

Fenton-like catalyst for sulfamethazine degradation. *Chemistry Engineering Journal, 375*, 122007. https://doi.org/10.1016/j.cej.2019.122007

Tang, X., Xue, Q., Qi, X., Cheng, C., Yang, M., Yang, T., Chen, F., Qiu, F., & Quan, X. (2022). DFT and experimental study on visible-light driven photocatalysis of rare-earth-doped TiO2. *Vacuum, 200*, 110972. https://doi.org/10.1016/J.VACUUM.2022.110972

Theerthagiri, J., Chandrasekaran, S., Salla, S., Elakkiya, V., Senthil, R. A., Nithyadharseni, P., Maiyalagan, T., Micheal, K., Ayeshamariam, A., Arasu, M. V., Al-Dhabi, N. A., & Kim, H. S. (2018). Recent developments of metal oxide based heterostructures for photocatalytic applications towards environmental remediation. *Journal of Solid State Chemistry, 267*, 35–52. https://doi.org/10.1016/J.JSSC.2018.08.006

Thevarajah, S., Huston, T. L., & Simmons, R. M. (2005). A comparison of the adverse reactions associated with isosulfan blue versus methylene blue dye in sentinel lymph node biopsy for breast cancer. *American Journal of Surgery, 189*, 236–239. https://doi.org/10.1016/J.AMJSURG.2004.06.042

Uribe López, M. C., Alvarez Lemus, M. A., Hidalgo, M.C., López González, R., Quintana Owen, P., Oros-Ruiz, S., Uribe López, A., & Acosta, J. (2019). Synthesis and characterization of ZnO-ZrO_2 nanocomposites for photocatalytic degradation and mineralization of phenol, *Journal of Nanomaterials*, *2019*, 1015876. https://doi.org/10.1155/2019/1015876.

Vaiano, V., Matarangolo, M., Murcia, J. J., Rojas, H., Navío, J. A., & Hidalgo, M. C. (2018). Applied Catalysis B: Environmental Enhanced photocatalytic removal of phenol from aqueous solutions using ZnO modi fi ed with Ag. *Applied Catalysis B Environmental, 225*, 197–206. https://doi.org/10.1016/j.apcatb.2017.11.075

Vickers, N. J. (2017). Animal communication: When I'm calling you, will you answer too? *Current Biology, 27*, R713–R715. https://doi.org/10.1016/J.CUB.2017.05.064

Viet, T. Q. Q., Khoi, V. H., Thi Huong Giang, N., Thi Van Anh, H., Dat, N. M., Phong, M. T., & Hieu, N. H. (2021). Statistical screening and optimization of photocatalytic degradation of methylene blue by ZnO–TiO_2/rGO nanocomposite. *Colloids Surfaces A Physicochemistry Engineering Asp, 629*, 127464. https://doi.org/10.1016/j.colsurfa.2021.127464

Vijaya Shanthi, R., Kayalvizhi, R., John Abel, M., & Neyvasagam, K. (2022a). Analysis on the combined effect of Gd^{3+} and Er^{3+} lanthanides in the microscopic, physicochemical and photocatalytic characteristics of MgO nanoparticles. *Option Material (Amst), 125*, 112118. https://doi.org/10.1016/J.OPTMAT.2022.112118

Vijaya Shanthi, R., Kayalvizhi, R., John Abel, M., & Neyvasagam, K. (2022). Optical, structural and photocatalytic properties of rare earth element Gd^{3+} doped MgO nanocrystals. *Chemistry Physical Letter, 792*, 139384. https://doi.org/10.1016/J.CPLETT.2022.139384

Wahba, M. A., Yakout, S. M., Mohamed, W. A. A., & Galal, H. R. (2020). Remarkable photocatalytic activity of Zr doped ZnO and ZrO_2/ZnO nanocomposites: Structural, morphological and photoluminescence properties. *Material Chemical Physical, 256*, 123754. https://doi.org/10.1016/J.MATCHEMPHYS.2020.123754

Wang, X., Yao, Z., Wang, J., Guo, W., & Li, G. (2008). Degradation of reactive brilliant red in aqueous solution by ultrasonic cavitation. *Ultrasonics Sonochemistry, 15*, 43–48. https://doi.org/10.1016/J.ULTSONCH.2007.01.008

Wang, B., Wei, K., Mo, X., Hu, J., He, G., Wang, Y., Li, W., & He, Q .(2019). Improvement in recycling times and photodegradation efficiency of core-shell structured Fe_3O_4@C-TiO_2 composites by pH adjustment. *ES Materials and Manufacturing*, *4*, 51–57. https://doi.org/10.30919/esmm5f

Wei, Y., Wang, J., Yu, R., Wan, J., & Wang, D. (2018). Constructing $SrTiO_3$-TiO_2 heterogeneous hollow multi-shelled structures for enhanced solar water splitting. *Angewandte Chemie*. https://doi.org/10.1002/ange.201812364

Wei, X. N., Ou, C. L., Guan, X. X., Peng, Z. K., & Zheng, X. C. (2019). Facile assembly of CdS-reduced graphene oxide heterojunction with enhanced elimination performance for organic pollutants in wastewater. *Applied Surface Science, 469*, 666–673. https://doi.org/10.1016/j.apsusc.2018.11.102

Wu, H., Tan, H. L., Toe, C. Y., Scott, J., Wang, L., Amal, R., & Ng, Y. H. (2020). Photocatalytic and photoelectrochemical systems: Similarities and differences. *Advanced Materials, 32*, 1–21. https://doi.org/10.1002/adma.201904717

Xiao, C., Li, J., & Zhang, G. (2018). Synthesis of stable burger-like a -Fe_2O_3 catalysts : Formation mechanism and excellent photo-Fenton catalytic performance. *Journal of Cleaner Production, 180*, 550–559. https://doi.org/10.1016/j.jclepro.2018.01.127

Xing, H. (2017). Syntheses of novel lanthanide metal – Organic frameworks for highly efficient visible-light-driven dye degradation. *Crystal Growth & Design*, *8*, 4189–4195. https://doi.org/10.1021/acs.cgd.7b00504

Xiong, J., Sun, Q., Chen, J., Li, Z., & Dou, S. (2016). Ambient controlled synthesis of advanced core-shell plasmonic Ag@ZnO photocatalysts. *CrystEngComm, 18*, 1713–1722. https://doi.org/10.1039/c6ce00013d

Xu, C., Ravi Anusuyadevi, P., Aymonier, C., Luque, R., & Marre, S. (2019). Nanostructured materials for photocatalysis. *Chemical Society Reviews, 48*, 3868–3902. https://doi.org/10.1039/c9cs00102f

Yagub, M. T., Sen, T. K., Afroze, S., & Ang, H. M. (2014). Dye and its removal from aqueous solution by adsorption: A review. *Advances in Colloid and Interface Science, 209*, 172–184. https://doi.org/10.1016/J.CIS.2014.04.002

Yan, X., Feng, J., Li, P., Li, J., Ren, B., Gao, S., & Cao, R. (2021). Fast and efficient removal of mercury ions using zirconium-based metal–organic framework filter membranes, Inorg. *Chemical Communications, 131*, 108796. https://doi.org/10.1016/J.INOCHE.2021.108796

Yang, Y., Jiang, K., Guo, J., Li, J., Peng, X., Hong, B., Wang, X., & Ge, H. (2020a). Facile fabrication of Au/Fe3O4 nanocomposites as excellent nanocatalyst for ultrafast recyclable reduction of 4-nitropheol. *Chemical*

Engineering Journal, 381, 122596. https://doi.org/10.1016/j.cej.2019.122596

Yang, X., Fu, H., Wang, W., Xiong, S., Han, D., Deng, Z., & An, X. (2020b). Enhanced solar light photocatalytic performance based on a novel Au-WO_3@TiO_2 ternary core–shell nanostructures. *Applied Surface Science, 505*, 144631. https://doi.org/10.1016/j.apsusc.2019.144631

Ye, Z., Padilla, J. A., Xuriguera, E., Brillas, E., & Sirés, I. (2020). Magnetic MIL(Fe)-type MOF-derived N-doped nano-ZVI@C rods as heterogeneous catalyst for the electro-Fenton degradation of gemfibrozil in a complex aqueous matrix. *Applied Catalysis B Environmental, 266*, 118604. https://doi.org/10.1016/j.apcatb.2020.118604

Yuan, X., Ge, H., Liu, X., Wang, X., Chen, W., Dong, W., & Huang, F. (2016). Efficient catalyst of defective CeO_{2-x} and few-layer carbon hybrid for oxygen reduction reaction. *Journal of Alloys and Compounds, 688*, 613–618. https://doi.org/10.1016/J.JALLCOM.2016.07.060

Yuan, Y., Wei, X., Yin, H., Zhu, M., Luo, H., & Dang, Z. (2022). Synergistic removal of Cr(VI) by S-nZVI and organic acids: The enhanced electron selectivity and pH-dependent promotion mechanisms. *Journal Hazardous Material, 423*, 127240. https://doi.org/10.1016/J.JHAZMAT.2021.127240

Zhang, Q. Q., Ying, G. G., Pan, C. G., Liu, Y. S., & Zhao, J. L. (2015). Comprehensive evaluation of antibiotics emission and fate in the river basins of China: Source analysis, multimedia modeling, and linkage to bacterial resistance. *Environmental Science and Technology, 49*, 6772–6782. https://doi.org/10.1021/acs.est.5b00729

Zhang, S., Zhang, Z., Li, B., Dai, W., Si, Y., Yang, L., & Luo, S. (2021). Hierarchical Ag_3PO_4@$ZnIn_2S_4$ nanoscoparium: An innovative Z-scheme photocatalyst for highly efficient and predictable tetracycline degradation. *Journal of Colloid and Interface Science, 586*, 708–718. https://doi.org/10.1016/j.jcis.2020.10.140

Zhang, S., Xu, Y., Zhang, W., & Cao, P. (2022b). Synthesis, characterization, and photocatalytic performance of Cu/Y co-doped TiO_2 nanoparticles. *Material Chemistry Physical, 277*, 125558. https://doi.org/10.1016/J.MATCHEMPHYS.2021.125558

Zhang, X., Jia, X., Xu, R., Lu, X., Liu, H., & Niu, Y. (2022c). Ellipsoidal α-Fe_2O_3@SnO_2/Ti_3C_2 MXene core-shell nanoparticles for photodegradation of organic dyes. *Journal Alloys Compoundd, 923*, 166315. https://doi.org/10.1016/j.jallcom.2022.166315

X. Zhang, X. Shi, Q. Zhao, Y. Li, J. Wang, Y. Yang, F. Bi, J. Xu, N. Liu, Defects controlled by acid-modulators and water molecules enabled UiO-67 for exceptional toluene uptakes: An experimental and theoretical study, Chem. Eng. J. 427 (2022a) 131573. https://doi.org/10.1016/j.cej.2021.131573.

Zhao, H., Zhang, G., Chong, S., Zhang, N., & Liu, Y. (2015). MnO_2/CeO_2 for catalytic ultrasonic decolorization of methyl orange: Process parameters and mechanisms. *Ultrasonics Sonochemistry, 27*, 474–479. https://doi.org/10.1016/j.ultsonch.2015.06.009

Zhong, Q., Lin, Q., Huang, R., Fu, H., Zhang, X., Luo, H., & Xiao, R. (2020). Oxidative degradation of tetracycline using persulfate activated by N and Cu codoped biochar. *Chemistry Engineering Journal, 380*, 122608. https://doi.org/10.1016/j.cej.2019.122608

Zhu, H. Y., Jiang, R., Fu, Y. Q., Li, R. R., Yao, J., & Jiang, S. T. (2016). Novel multifunctional $NiFe_2O_4$ /ZnO hybrids for dye removal by adsorption, photocatalysis and magnetic separation. *Applied Surface Science, 369*, 1–10. https://doi.org/10.1016/j.apsusc.2016.02.025

Zong, Y., Li, Z., Wang, X., Ma, J., & Men, Y. (2014). Synthesis and high photocatalytic activity of Eu-doped ZnO nanoparticles. *Ceramics International, 40*, 10375–10382. https://doi.org/10.1016/J.CERAMINT.2014.02.123